AERODYNAMICS OF WIND TURBINE WITH TOWER DISTURBANCES

by

SONG Y. CHUNG

B.S., Seoul National University
(1975)

SUBMITTED IN PARTIAL FULFILLMENT
OF THE REQUIREMENTS FOR THE
DEGREE OF MASTER OF SCIENCE

at the

MASSACHUSETTS INSTITUTE OF TECHNOLOGY

June, 1978

Signature of Author Signature redacted
Department of Aeronautics and Astronautics
January 30, 1978

Certified by Signature redacted
Thesis Supervisor

Accepted by Signature redacted
Chairman, Departmental Graduate Committee

AERODYNAMICS OF WIND TURBINE WITH

TOWER DISTURBANCES

by

SONG YOUNG CHUNG

Submitted to the Department of Aeronautics and Astronautics on May 30, 1978, in partial fulfillment of the requirements for the degree of Master of Science

ABSTRACT

Lifting line theory which is the counterpart of Prandtl's lifting line theory for rotating wing is employed for the overall performance analysis of a horizontal axis wind turbine rotor operating in a uniform flow. The wake system is modeled by non-rigid wake which includes the radial expansion and the axial retardation of trailing vortices.

For the non-uniform flow which are caused by the ground, the tower reflection, or the tower shadow, the unsteady airloads acting on the turbine blade are computed, using lifting line theory and a non-rigid wake model. An equation which gives the wind profile in the tower shadow region is developed. Also, the equations to determine pitch angle control are derived to minimize the flapping moment variations or the thrust variations due to the non-uniform flow over a rotation

It is concluded that the models developed can predict the overall performance coefficients for uniform flow and the unsteady airloads for non-uniform flow which are in good agreement with experimental data. The unsteady airloads are found to have the same form variations as the wind profile on the rotor disk plane.

Thesis Supervisor; Rene Harcourt Miller

Title: Slater Professor of Flight Transportation

Head of Department of Aeronautics and Astronautics

ACKNOWLEDGEMENTS

My sincere gratitude is directed to Professor R.H. Miller for his continuing advice and supervision throughout all of this research. Without his many invaluable suggestions and comments, as well as his encouragements this thesis could not have been completed. I would like thank Mr. Thomas Matoi for his helpful discussions and advice during the past year.

This research has been supported by the U.S. Energy Research and Development Administration under contract No.E(11-1)-4131.

NOMENCLATURE

a	lift curve slope
A_j	coefficients of bound circulation series ($\Gamma = \Sigma A_j \sin \cdot j\theta$)
b	number of blades
c	blade chord
C_d	drag coefficient of blade
C_{dt}	drag coefficient of the tower
C_p	power coefficient, $C_p = P/\rho \pi R^2 U_\infty^3$
C_T	thrust coefficient, $C_T = T/\rho \pi R^2 U_\infty^2$
dL	lift per unit length of blade
e	flapping hinge offset
G	$(\omega_{pend}/\Omega)^2$ where $\omega_{pend} = \sqrt{3g/2\ell R}$ is pendulum frequency of blade
i	index to denote control point
I_b	blade moment of inertia
K_1, K_2	characteristic constants of wind profile equation for a given tower
K_β	root constraint
ℓ	distance from hinge offset to blade tip nondimensioned by R
LN	lock number, $LN = ac\rho R^4/I_b$
L_T	thrust coefficient, $L_T = T/\rho\pi\Omega^2 R^4$
L_{Tn}	coefficients of thrust coefficient series
$\dot{m}$	mass per unit length of blade
M_A	aerodynamic moment about an offset flapping hinge
M_g	moment due to gravity about an flapping hinge
M_I	inertia moment about an flapping hinge
$M_{\dot{\beta}}$	$= \frac{LN}{8} \ell^4 (1 + \frac{4e}{3\ell})$

R	rotor radius
$\vec{r}$	position vector from vortex element to point where induced velocity is going to be computed
r_t	radius of the tower
S	static unbalance of blade
$\vec{s}$	position vector from center of coordinate to vortex element
u^*	free stream velocity on rotor disk plane disturbed by tower
U	total velocity on blade
U_p	velocity perpendicular to rotor disk plane
U_T	in-plane velocity perpendicular to blade
U_∞	undisturbed free stream belocity
U_i	total velocity at i-th control point
v	velocity reduction function
V^*	inflow velocity, $V = U_p/\Omega R$
W^*	induced velocity perpendicular to rotor disk plane
W_x^*	in-plane induced velocity
W_r^*	radial induced velocity
W_{r0}^*	radial induced velocity on rotor disk plane
α	angle of attack
β	rigid body flapping angle
β_n	coefficients of rigid body flapping angle series
Γ_{AV}	average bound circulation over a rotation
Γ_i	bound circulation at i-th control point
$\Delta\Gamma_D$	half of maximum bound circulation variation over a rotation
η	spanwise coordinate (non-dimensioned by R)
η_{rc}	non-dimensional distance from center of rotation to blade root cut
$*$	non-dimensioned by ΩR

Θ angular coordinate to denote spanwise position

Θ_n coefficients of blade pitch angle series

Θ_p blade pitch angle

λ inflow angle

λ_i induced inflow angle ($\cong w/\eta$)

λ_a absolute inflow angle ($\cong U_\infty/\eta$)

ρ density of air

μ advence ratio

ν kinematic viscosity of air

σ solidity, $\sigma = \pi R/bc$

ϕ azimuthal angular coordinate of vortex element from blade

ϕ_n phase angle between flapping angle series and inflow angle series

ϕ'_n phase angle between pitch angle series and inflow field series

Ψ azimuthal angular coordinate

Ω rotational speed of wind turbine rotor

TABLE OF CONTENTS

SECTION 1

INTRODUCTION

For uniform steady flow about a wind turbine, lifting line theory which is the counterpart of the Prandtl's lifting line theory for rotating wing is employed in the analysis for a rotor blade in an effort to improve the theoretical prediction of power and thrust. The wake region is divided into three regions, namely, the near, intermediate , and far wakes. At the junction between the near and intermediate wakes, the neighboring two vortices are merged together. Again, at the junction between the intermediate and the far wakes, all trailing vortices are assumed to be rolled-up into the root and tip vortices. The wake geometry is prescribed at equal angle spacings and the blade is divided into a number of segments according to cosine law. Each segment is represented by a constant strength bound vortex whose strength is determined at a control point which is located at equal angle center of that segment. The wake geometry used in the analysis includes the linearly varying velocities induced on the tip or root vortex in the first spiral and the radial movement of them. The results obtained with this wake geometry are compared with those obtained with the semi-rigid wake assumption. The computer program for the steady flow analysis permits the evaluation of several wake geometries ranging from the classical helicoids, the semi-rigid wake to the radially expanded, variable-axial-velocity geometry. The inboard trailing vortices may be unrolled or fully rolled in the last two wake geometries.

The importance of the correct axial and radial positioning

of the tip vortex was noticed in ref.[4]. The disagreement of the theoretical predictions using the classical wake geometry with experimental results is mainly due to the neglect of the rapid contraction of the slipstream under a hovering rotor which places the vortex system close to the rotor blades[4]. The free wake analysis was introduced in [14] to account for the significance of blade wake interference and the influence of blade number. The cross section view of the calculated wake geometry (ref.14) shows that the outer end of the vortex system, that is, the vortex emanated at blade tip becomes the center of the rolled-up concentrated tip vortex.

For the unsteady nonuniform flow which is inevitable due to wind shear, and tower reflection or tower shadow, the non-linear variable-axial-velocity induced on the tip or root vortices are computed for each azimuthal increment within the first spiral. The calculations show that the velocity induced on the tip vortex increases sharply and is almost doubled within the first spiral. After that induced velocity remains relatively unchanged. This means that the retardation of the tip vortex occurs and momentarily it expands behind the rotor. This radial expansion is computed from the condition of constant mass flow inside the cylinder bounded by the tip vortex. Tower effect is included in the analysis through the nonuniform flow field on the rotor disk plane caused by the tower reflection or its shadow. The distortions of the trailing vortex system due to this nonuniform flow is, also, included. But in the tower reflection case, the vortex-tower interaction is

neglected because it occurs after several spirals of the tip vortex. The shed vortex lines in the far wake are positioned by the connecting lines of the points determined by the velocities induced on the two control points near the tip or the root. In the rigid or semi-rigid wake the shed vortex was located by the tip and root vortices. The trailing vortices are permitted to have varying directions and strengths.

The equations are derived to determine the blade pitch angle required to minimize the flapping moment variations, or the thrust variations over a rotation. All blade are assumed to be rigid. For the tower shadow case the rigid body flapping angle is calculated and its effects are evaluated.

Miller, R.H. in [2] has pioneered the unsteady harmonic airload computation for the forward flight of the helicopter with rigid wake geometry. Unsteady airloads acting on rotor blades were predicted satisfactory and their orgins were discussed in [1] and [3]. The concept of the semi-rigid wake geometry was introduced in those reports. Scully, M.P. in [6] has done the free wake analysis for the helicopter forward flight, where the induced velocities on the first two spirals of the tip vortex were computed in order to locate the tip vortex and the inboard shed wakes were positioned by the rigid wake geometry.

SECTION 2

STEADY AERODYNAMICS

The bound circulation which describes the blade as a lifting line is represented by a Fourier sine series. The velocities induced by the prescribed wake are computed at control points on the blade as a function of the coefficients of the bound circulation series. These coefficients are calculated from the matrix equation which are formed according to the Kutta-Joukowsky theorem. The multiplication of these coefficients with the influence coefficients yields the induced velocities on the blade. From these non-uniform induced velocities and the free stream velocity the wake is generated within the framework of the assumed geometry. New influence coefficients, induced velocities and bound circulation are obtained from this new geometry. This procedure is usually iterated three times to get the converged bound circulation and induced velocities. The usual strip analysis gives the performance coefficients of the wind turbine.

2.1 Lifting Line Theory

Bound circulation along the blade is represented as a sine series. The velocity induced at each control point on the blade by the wake system is computed as a function of the coefficients of the bound circulation harmonic series. Then, the induced angle of attack is obtained at each control point as a function of those coefficients. The angle of attack calculation also includes contributions from the pitch angle, the rotational velocity

of blade and the free stream velocity.

All of the above contributions are included in lifting line equation at each control point, which generates a system of linear algebraic equations for the coefficients of bound circulation series as follows. The sectional lift at a control point on the blade is given by Kutta-Joukowsky theorem.

$$dL = \rho U \Gamma = \frac{1}{2} \cdot \rho \cdot U^2 \cdot a \cdot \alpha \cdot C \qquad (2.1)$$

Here, $\alpha = \Theta_p + \lambda_a + \lambda_i$ as shown in fig.2.1 .

$$w_i = \sum_{j=1}^{N} A_j \cdot C_{ij} \qquad (2.2)$$

$$\Gamma = \frac{1}{2} U a C (\Theta_p + \lambda_a + \lambda_i) \qquad (2.3)$$

The influence coefficients C_{ij} are computed from the equation derived in the appendix. A_j is the coefficients of bound circulation series, that is,

$$\Gamma_i = \sum_{j=1}^{N} A_j \sin (j \cdot \Theta_i) \qquad (2.4)$$

N is the number of control points on the blade

The spanwise coordinate on the blade, η_i, is transformed into a polar coordinate, Θ_i , which varies from 0 to π according to the following transformation equation

$$\eta_i = \eta_{rc} + 0.5 (1 - \cos \Theta_i)$$

(See fig. 2.2 for details.)

During the intermediate calculations every value was non-dimensioned by the distance from the rootcut to the blade tip. In the

final output the non-dimensional parameter was switched to the blade radius. Introduction of equations (2.2) and (2.4) into (2.1) gives the desired linear algebraic equation for the coefficients of circulation.

$$\sum_{j=1}^{N} A_j \sin(j\cdot\Theta_i) = \frac{1}{2} U_i \cdot a_i \cdot C_i \left\{ \Theta_{pi} + \lambda_{ai} + \left(\sum_{j=1}^{N} A_j C_{ij} \right) / \eta_i \right\}$$

$$\sum_{j=1}^{N} A_j \left[\sin(j\cdot\Theta_i) - \frac{1}{2} U_i \cdot a_i \cdot c_i \cdot C_{ij} / \eta_i \right] = \frac{1}{2} U_i \cdot a_i \cdot C_i (\Theta_{pi} + \lambda_{ai})$$

$$\sum_{j=1}^{N} A_j \alpha_{ij} = D_i$$

This equation is valid at each control point (i). Therefore, it gives the following matrix equation.

$$[\alpha_{ij}]\{A_j\} = \{D_i\}$$

$$\{A_j\} = [\alpha_{ij}]^{-1}\{D_i\} \qquad (2.5)$$

Here, in-plane induced velocities were neglected because the effect of these velocities on the results was shown to be negligible in [7].

In generating equation (2.5), U_i is a function of induced velocity and C_{ij} is a function of wake geometry which is determined from induced velocity distribution within the assumption for geometry. That means an iterative procedure, as described below, must be employed to compute the actual A_j.

Iteration Procedure

1. Estimate induced velocities
2. Calculate U_i

3. Generate wake geometry

4. Calculate influence coefficients C_{ij}

5. Solve equation (2.5)

6. Calculate induced velocities from equation (2.2)

7. Repeat step 2-6 untill the solution converges

Knowing the proper induced velocities a strip analysis is used in calculating the thrust and power distribution. Experimental data for section lift slope and drag can be used. Wind turbine rotor in this analysis can have any number of blades which can have an arbitrary distribution of taper and twist.

Ref.[9] applied the vortex lattice method to propeller blades with a single bound vortex located at the quarter-chord point and the control point at the three-quarter chord point of each blade section. For non-rotating rectangular wing [8] shows that lifting line theory with trailing vortices arranged by equal angle distance and control point at the equal center between them converges faster and is more accurate than other vortex lattice methods.

2.2 Wake Geometry

The prescribed wake geometry resulting from a series of investigations of model rotor wakes was successfully applied to the calculation of helicopter rotor hover performance with lifting line theory in [4] and lifting surface theory in [5]. At the present time, there is no wake geometry available for the wind rotor which has been developed from such experimental studies.

Hence,two major features from the prescribed wake geometries for helicopter rotor hover performance analysis are incoperated in the calculation of wake geometries.

First, the tip vortex axial settling rate (or velocity) was doubled when the tip vortex passes beneath the following blade. This doubling is predicted by momentum theory and in vortex theory can be explained by the effect from the trailing and bound vortex system of that blade generated during that portion of the cycle preceeding the following blade passage. For wind turbine rotor there is the same effect on the tip vortex from the following blade's trailing and bound vortex system. Also, the equation derived in [12] show that the thrust predicted by simple vortex theory for the rotor with an infinite number of blades will be equal to that estimated by momentum theory when the axial induced velocity on the tip vortex is taken over the rotor disk.

The second feature is that the point of maximum wake contraction is reached at the end of four times the azimuthal angle between adjacent blades[10,11] In the analysis the maximum wake expansion point for the wind turbine rotor is taken to be the maximum wake contraction point for the helicopter rotor.

The radial induced velocity (W_{r0}) at the blade tip on rotor disk plane is computed as follows. The tip vortex begins to move radially with that velocity when it is trailed from the blade. It is assumed that the tip vortex radial velocity decreases linearly to zero when it reaches the assumed maximum expansion point. Therefore, the radial velocity of tip vortex is

$$w_r = w_{ro} - \frac{\phi}{(8\pi/b)} \cdot w_{ro} \qquad (2.6)$$

where w_{ro} is the radial induced velocity at the blade tip in the rotor disk plane, b is the number of blade and ϕ is the azimuthal position of vortex. The maximum expansion distance is given as follows for b = 2.

$$d(\phi) = w_{ro}\phi - \frac{\phi^2}{8\pi} \cdot w_{ro}$$

$$d_{max}(\phi = 4\pi) = 2\pi\, w_{ro} \qquad (2.7)$$

The radial movement of tip vortex is due to the radial velocity induced by the spiral tip vortex below the rotor disk plane as shown in fig. 2.3 . In fig. 2.3 the radial velocity of tip vortex, C is decreased due to the radial velocity induced by the vortices trailed since tip vortex C had been trailed, that is, vortices A and B. The tip vortex moves radially until the radial velocity induced by the almost helical vortex below that vortex is balanced by the radial velocity induced by the spiral vortex above it. After the tip vortex reaches its maximum expansion point, it begins to contract much more slowly than when it expands just below the rotor disk plane. This is due to the fact that the radial velocity induced by the lower helical vortex ceases to dominate over the velocity induced by the upper sprial vortex because of wake diffusion due to the viscous effects. Since this tip vortex begins to contract relatively far below the rotor disk plane and very slowly, its effect on performance and thrust can be neglected. Experimental investigation in [11] shows for helicopter hovering rotor that the

wake system contracts first and then expands very slowly.

This radial movement of rolled-up tip vortex has a fairly large effect on power results because the axial velocity of tip vortex is influenced by the radial position of tip vortex and the induced velocity near blade tip is affected very much by the axial and radial position of rolled-up tip vortex. The axial induced velocity of rolled-up tip or root vortex is computed under the scheme that the vortex originating at the blade tip or root cutout becomes the center of the rolled-up tip or root vortex and that the vortices trailed from the maximum-bound-circulation point to the tip or the rootcut are warpped around those center vortices. Concentrated tip or root vortices are explained to be caused by a very high slope drop toward zero of the bound circulation ($d\Gamma/dy = \infty$) on those points. These concentrated vortices tend to induce strong velocity around them and to make the neighboring vortex sheet warp around them. Therefore, the rolled-up vortex moves with the velocity which is the sum of the undisturbed free stream velocity and the induced velocity at the blade tip or rootcut. The velocity induced on the tip or root vortex is assumed to increase linearly until it is doubled when it passes underneath the following blade as discussed above.

The wake system is usually divided into three regions, near, intermediate, and far wake. At the junction between the near and the intermediate wakes the number of trailing vortices is cut in half by merging two adjacent trailing vortices into one. All trailing vortices are assumed to be rolled-up into the root or tip

vortex at the junction point between the intermediate and far wakes. The velocity induced by the intermediate and the far wakes is computed at the blade tip or the rootcut point. But the velocity induced by the near wake is computed by averaging the velocities induced at two points outside and inside the blade tip or rootcut. In semi-rigid wake the induced velocity at the tip or the root cut is taken as the half of the velocity induced at the nearest control point. For a rotor of an infinite number of blades the induced velocity at the tip was shown to be the half of the velocity induced at inboard station of the tip in [12] .

SECTION 3

UNSTEADY AERODYNAMICS

Wind turbines always operate in the influence of their towers and the ground. The unsteady airloads act on the wind turbine blades which rotate through the non-uniform flow field caused by these influences. The calculations of these unsteady airloads have been performed by the vortex wake and lifting line theory, which means the lifting blade is modeled by a bound circulation and the chordwise circulation variation is neglected. The wake geometry employed is the non-rigid wake which includes the effects of the retardation of trailing vortices and of the radial movement of the tip vortex. This geometry is calculated from the semi-rigid wake geometry by suitable and systematic modifications. In this non-rigid wake the shed vortex lines in the far wake are placed on a plane other than the one defined by the rolled-up tip or root vortices because the induced velocities on those vortices are entirely different from the induced velocities inboard of them.

The influence of the tower on the vortex wake system have been included on the rotor disk plane. These vortex wakes are positioned by the timewise integration of the velocities which are the sum of the disturbed velocities on the rotor disk plane due to the tower and the velocities induced on vortex itself. But in the tower reflection case when vortices approach the tower the free stream velocities are decreasing and there are interactions between the vortex system, especially the tip vortex and the tower. It may happen after several spirals that the tip vortex will

touch the tower and end on the solid boundary because of the decrease of the free stream velocity and the vortex-tower interactions. The effect of this phenomena on the induced velocities have been neglected because the contact of the tip vortex with the tower will usually take place after several spirals. Hence its effect will be negligible, compared to the velocities induced by the several spirals of the tip vortex before the contact happens.

The blade are assumed to be rigid. The rigid body flapping motion is determined for the tower shadow case and its effect on the unsteady airloads are discussed.

The equation which gives the wind profile downwind of the tower has been developed by using boundary layer approximations. That equation is shown to be a good characterization of the wind profile downwind of the tower.

3.1 Wind Turbine Blades

All blades are assumed to be identical, to rotate at a constant angular velocity, and to have arbitrary twist distribution. The tower and blades are assumed to be rigid. Each blade is represented by a number of constant-strength bound virtex segments which have the bound circulation that is determined by two-dimension airfoil theory at their mid-point. The same method as used in [7] is used for the modeling of the blades.

3.2 Wakes

The wakes consists of trailing vortices and shed vortices as shown in fig. 3.1 which are caused by the spanwise and azimutal variations of bound circulation and are divided into near, intermediate, and far wake regions. The near wake region extends from the blade to 15 degrees aft and has three 5 degree sections. It has been modeled by curved trailing vortex elements having varying strengths and varying directions within one element and lattice vortex sheet elements each of which has constant strength and direction. The same procedure as the one in [7] has been followed in dividing the wake regions and determing the strengths of vortices.

3.3 Non-rigid Wake Geometry

The semi-rigid wake usually assumes that the vortices shed from the blade are carried away from the rotor at a rate equal to the relative velocity of the flow passing through the rotor. These velocities are in general different at different points of this flow. Also, the vortex system is continuously being deformed due to these different velocities and the mutual interactions of the tip vortices. As a result, the velocity with which the tip or root vortex carried away from the rotor plane is radically different than the velocities on the inboard sheet vortices. The vertical transport velocity of the outer portion of these sheets is much lower than that of the tip vortices.

If we consider the vertical transport velocity of one tip vortex element, the assumption made in the usual semi-rigid wake

is roughly equal to neglecting the interaction by the vortex segments shed after the tip vortex element was shed. Let the velocity with which the element A in fig.3.2A is carried away be V_A. When one tip vortex element A is trailed, the vertical transport velocity V_A becomes

$$V_A = V + W_a = V + \sum_b \int_{\phi=0}^{\phi=\infty} \frac{d\Gamma}{d\eta} \frac{\vec{ds} \times \vec{r}}{4\pi r^3} d\eta$$

where b is the number of blades, if the shed wake is neglected. If we consider that vortex element after the time interval, $\Delta t = \phi_o/\Omega$, it is positioned as shown in fig. 3.2B. The vertical velocity of the element A at position Q becomes

$$V_A = V + W_a' + W_b + W_\Gamma$$

$$W_a' = \sum_b \int_{\phi=\phi_o}^{\phi=\infty} \int_o^1 \frac{d\Gamma(\eta,\phi)}{d\eta} \frac{\vec{ds} \times \vec{r}}{4\pi r^3} d\eta$$

$$W_b = \sum_b \int_{\phi=0}^{\phi=\phi_o} \int_o^1 \frac{d\Gamma(\eta,\phi)}{d\eta} \frac{\vec{ds} \times \vec{r}}{4\pi r^3} d\eta$$

$$W_\Gamma = \sum_b \int_o^1 \Gamma(\eta,\phi) \frac{\vec{d\eta} \times \vec{r}}{4\pi r^3}$$

W_a' is the velocity induced at point Q by the vortex system trailed from the blade before the vortex element A was trailed. It can be reasonably assumed that W_a' is equal to W_a. If one considers the wind turbine to have more than one blade, average W_Γ is almost

cancelled. But actually the instantenous velocity induced at point Q by the bound circulation is not cancelled.

The most important factor which invalidates the assumption made in usual semi-rigid wake is W_b. At $\phi_o = 15^\circ$, W_b is of the order of 40 % of the velocity induced at point P by W'_a. After one spiral W_b is almost equal to 70 % of W'_a. Therefore the usual semi-rigid wake assumption causes us to underestimate the induced velocity at the blade, especially near the blade tip. As a result, the performance of the wind turbine is overestimated for a given pitch angle. In helicopter hovering case, the situation is reversed.

The velocity induced at Q by the vortex segment B in fig. 3. 2B causes the retardation of vortex element A. **The tip vortex trailed by the preceding blade therefore passes near the following blade,** but not as in helicopter forward flight rotor case because this tip vortex goes a little outside of the following blade tip. This tip vortex increases the induced velocity near the blade tip, comared to the usual assumption.

In the calculation of velocities induced at the blade by its wake system, the usual semi-rigid wake assumption is used in the near wake region. In intermediate and far wake regions, the velocity V_A of the vortex element A which was trailed when the blade was at P is modified by the velocity induced by vortex elements trailed by the blade since its orgin. The contributions of these regions are similarily divided into near, intermediate, and far wake regions for the point A. The near wake contribution is obtained from the near wake contribution when the blade was at point P and is thus not

recomputed. Similarly the intermediate and far wake contributions are obtained from the corresponding regions for the point P'. After the first spiral of the wake, V_A is assumed to keep the velocity obtained according to the above procedure since the contributions of the remaining spirals will have a negligible effect on this geometry. The axial distance of element A in fig. 3.2B from the rotor disk plane is calculated by integrating the changing V_A w.r.to the time interval corresponding to the various induced velocities on element A. The radial location of the tip vortex is established by satisfying the equation of continuity for the flow inside the vortex spiral.

This scheme does not need any more difficult steps to calculate the wake geometry than for the usual assumption made in semi-rigid wake. To reduce execution time and avoid some useless calculations, the calculation of the velocity induced by the shed or trailing wake element was not performed, if the strength, $\left|\frac{d\Gamma}{d\phi}\Delta\phi\right|$ or $\left|\frac{d\Gamma}{d\eta}\Delta\eta\right|$ was less than the corresponding reference* values. In far wake after 6 spirals, the velocities induced by the half vortex system nearest the blade are calculated and those induced by the other half are neglected.

3.4 Calculation of Non-linear Movement of the Vortex

The tip vortex decelerates and expands quickly in the first spiral after it was trailed. After the first spiral it maintains almost constant pitch and radial distance from the rotor axis. When the blade passes above the rolled-up tip vortex trailed from the preceding blade, that vortex plays a determinate role on the velocity at the blade tip, and consequently on the performance of the

* $\frac{1}{1000}$ of mean value of Γ

wind turbine. Thus, the correct position of that vortex with respect to the blade is required. All these considerations necessitate the introduction of the calculation of the non-linear movement of the tip vortex in the first spiral. This calculation is done in a relatively simple way.

The non-linear movement of the near wake is neglected, since the age of the near wake after it was trailed is negligible so that any departure from a linear movement is insignificant. In fig. 3.3 the axial velocity V_L of tip vortex element L is

$$V_L = V_{0L} + \sum_{K=1}^{L-1} W_{L,K} \qquad (3.1)$$

where $W_{L,K}$ is the velocity induced at the element L by the element K and V_{0L} is the starting velocity of element L at that instant when the blade is located at the azimuthal angle Ψ_L. The axial distance H_L of element L is

$$H_L = V_{0L} \cdot \phi_L + \sum_{K=1}^{L-1} W_{L,K} \cdot \Delta\phi \cdot K \qquad (3.2)$$

,where ϕ_L is the azimuthal angle between element A and the current blade position and $\Delta\phi$ is the angular interval between the vortex elements. The calculation of $W_{L,K}$ for each vortex element L is very time consuming. Without actually computing $W_{L,K}$ it is obtained from th velocity which is induced by each vortex element L at the blade tip.

$$W_{L,K} = W_{N,L-K} \cdot \frac{\Gamma_t(K)}{\Gamma_t(L-K)} \qquad \text{for } 1 \leqq K \leqq L-8 \qquad (3.3)$$

Here, $\Gamma_t(K)$ is the strength of the vortex element K and $W_{N,L-K}$

is the velocity induced at the blade tip (η_N) by the vortex element L-K. $W_{L,L-7}$, ... , $W_{L,L-2}$ are again obtained from the velocity induced at the blade tip by the intermediate wake and $W_{L,L-1}$ from the velocity induced by the near wake.

The position of the shed line vortex in the far wake is defined by the line connecting two positions which are determined by the sum of the free stream velocity and the velocities induced at η_2 and η_{N-1} in fig. 3.3. Using the same method which was used to position the tip and root vortices, the relations (3.1) to (3.2) are employed while $W_{N,L-K}$ is replaced by $W_{2,L-K}$ in order to locate the inboard end of the shed line vortex and by $W_{N-1,L-K}$ in order to locate the outboard end of that line vortex. The radial position of the tip vortex is computed from the condition of constant mass flow inside the vortex cylinder.

The axial velocity at the rolled-up tip or root vortex is computed according to the scheme that the vortex originating at the blade tip or rootcut becomes the center of the rolled-up tip or root vortex and the vortices trailed from the maximum-bound-circulation point to the tip or the rootcut are wrapped around that center vortex. Therefore, the rolled-up vortex moves with velocity which is the sum of the undisturbed free stream velocity and the induced velocity at the blade tip or rootcut and its axial velocity changes are computed in the manner explained above. The velocity induced at the tip or rootcut by the near wake is computed in the same manner as discussed in section 2.2 . The velocity induced by the intermediate and far wakes is computed at the blade

tip or the rootcut point itself.

3.5 Effect of the Up-wind Tower Presence on the Wind Approaching the Rotor Disk Plane

The dirrect effect of the presence of the tower is the continual spreading of the wake. The velocity distribution in the wake is likely to be complicated in the neighborhood of the tower, even when the flow is steady. Farther downstream in a steady wake the vorticity shed from the tower is convected in the stream direction and diffused by viscosity. In this region the boundary layer approximations are applicable asymptotically. Thus, assuming that the flow downstream of the tower is a steady two dimensional wake, the governing equation of motion is

$$U_\infty \left(\frac{\partial u}{\partial x}\right) = \nu \left(\frac{\partial^2 u}{\partial y^2}\right) \tag{3.4}$$

and the boundary condition at the edge of the wake is $u \longrightarrow U_\infty$ as $y \longrightarrow \infty$. Ref. [15] gives the asymptotic solution for equation (3.4).

$$U_\infty - u \longrightarrow Q\sqrt{\frac{U_\infty}{4\pi\nu x}}\; e^{-\frac{U_\infty y^2}{4\nu x}} \qquad \text{as} \quad x \longrightarrow \infty$$

Here, x is the downstream distance from the tower center to the rotor disk plane and y is the lateral distance from the tower center to the position of interest in the rotor disk plane. Q is

a constant determined by $Q = D_t/\rho U$ where D_t is the drag of the tower.

Let the velocity reduction function, v, be defined as follows.

$$v = \frac{U_\infty - u}{U_\infty} = Q \frac{1}{\sqrt{4\pi\nu x U_\infty}} e^{-\frac{U_\infty}{4\nu x} y^2} \tag{3.5}$$

$$D_t = \rho U_\infty Q = \frac{1}{2} C_{dt} \rho U_\infty^2 A$$

$$Q = \frac{1}{2} \cdot C_{dt} \cdot U_\infty^2 \cdot r_t = C_{dt} \cdot U_\infty \cdot r_t \tag{3.6}$$

where r_t is the radius of the tower. The introduction of equation (3.6) into (3.5) yields

$$v = C_{dt} \frac{1}{\sqrt{4\pi\nu x}} r_t \sqrt{U_\infty}\, e^{-\frac{1}{4\nu x} U_\infty y^2}$$

$$= K_1 r_t \sqrt{U_\infty}\, e^{-K_2 \cdot U_\infty y^2} \tag{3.7}$$

$$K_1 = f(C_{dt}, \nu, x), \quad K_2 = f(\nu, x)$$

K_1 and K_2 can be considered as chacteristic constants for a given tower which depends on the tower and the downstream distance from tower to the rotor disk plane. In the present analysis K_1 and K_2 are obtained by comparing the tipical experimental wind profile with equation (3.7).

SECTION 4

SIMPLE BLADE DYNAMICS

The harmonic analysis of the blade flapping motion was done in order to get an idea of the effect of the blade motion on the airloads. This flapping motion is caused by a change in the circulation of the lifting blade due to disturbance of the flow field by the tower. Cylic changes in the aerodynamic flapping moment of the blade and in the force acting on the tower are caused by the changes in the blade lift. These cylic changes are undesirable in view of the fact that the flapping motion can give rise to severe vibrational problems, vibrations coupled with the other motions of the blade and with the tower vibrations. The periodically varying blade thrust acts on the tower as a cyclic external force and a varying torque.

The equation for moment equilibrium about an offset flapping hinge is derived to determine the coefficients of the flapping motion series, given the known disturbed flow field due to the presence of the tower and the induced flow field. Based on the series representation of the inflow field(V) on the rotor disk plane, equations are derived to determine the pitch angle control which can minimize the flapping moment variation or the thrust variation over a rotation. The minimization of the rigid body flapping motion is equivalent to minimizing the flapping moment variations over a rotation because $k_\beta \beta$ is equal to the flapping moment acting on the offset hinge.

4.1 Harmonic Analysis of Blade Flapping Motion

Considering the rigid flapping motion about an offset hinge , the blade flapping moment equilibrium gives the flapping equation of motion.

$$M_A + M_I + M_g = K_\beta \cdot \beta \qquad (4.1)$$

where M_A= flapping moment due to aerodynamic force

M_I= flapping moment due to inertia force

M_g= flapping moment due to gravity

K_β= root constraint

M_A , M_I ,and M_g are derived as follows. (See fig. 4.1 for details)

$$dM_I = -r\ddot{\beta}\, \dot{m}\, r\, R^3\, dr - \Omega^2 R^3 (r + e)\, r\beta\, \dot{m}\, dr$$

$$M_I = \int_0^{\ell R} dM_I = -\left[I_b \ddot{\beta} + \left(I_b + I_b \frac{3}{2}\frac{e}{\ell} \right) \Omega^2 \beta \right] \qquad (4.2)$$

$$dM_A = L(r, \psi)\, R^2\, r\, dr$$

with $$L(r, \psi) = \frac{1}{2} \rho a c\, U^2(r, \psi)\, \alpha(r, \psi)$$

where $$\alpha(r, \psi) = \Theta_p(r, \psi) + \tan^{-1}(U_p/U_T)$$

$$U_T/\Omega R \cong (r + e)$$

$$U_p/\Omega R = w(r, \psi) - r\dot{\beta} + u(r, \psi)$$

$$U^2 = U_T^2 (1 + U_p^2/U_T^2) \cong U_T^2$$

$$\tan^{-1}(U_p/U_T) \cong U_p/U_T$$

These approximations are valid for the usual operating conditions of high tip speed ratio.

Then, $$M_A = \frac{I_b \Omega^2 LN}{2} \int_0^{\ell} r \left[\Theta_p (r, \Psi) (r + e)^2 + V(r, \Psi) (r + e) \right] dr - \frac{LN}{8} I_b \Omega \ell^4 \left(1 + \frac{4e}{3\ell}\right) \dot{\beta} \qquad (4.3)$$

$$dM_g = R^2 \dot{m} g \cos\Psi \cdot r \cdot \beta \cdot dr$$

$$M_g = g \beta \cos\Psi \cdot S \qquad (4.4)$$

In these expressions,

$$\left.\begin{aligned} I_b &= \frac{1}{3} \dot{m} (\ell R)^3 \\ LN &= ac \rho R^4 / I_b \\ M_{\dot{\beta}} &= \frac{LN}{8} \ell^4 \left(1 + \frac{4e}{3\ell}\right) \\ S &= \frac{1}{2} \dot{m} (\ell R)^2 \end{aligned}\right\} \qquad (4.5)$$

Substitution of the equations (4.2), (4.3) and (4.4) into equation (4.1) yields the flapping equation of motion.

$$I_b \ddot{\beta} + I_b \Omega M_{\dot{\beta}} \dot{\beta} + I_b \left(1 + \frac{3}{2} \frac{e}{\ell}\right) \Omega^2 \beta + K_\beta \beta - g S \cos\Psi \cdot \beta = \frac{I_b \Omega^2 LN}{2} \int_0^{\ell} r \left[\Theta_p (r, \Psi) (r + e)^2 + V(r, \psi) (r + e) \right] dr \qquad (4.6)$$

Switching the independent variable from time to azimuthal angle (Ψ) renders the final flapping equation.

$$\ddot{\beta} + M_{\dot{\beta}} \dot{\beta} + \nu_\beta^2 \beta - G \cdot \cos\psi \cdot \beta = \frac{LN}{2} \int_0^{\ell} \left[\Theta_p (r, \psi) \cdot r \cdot (r + e)^2 \right.$$

$$+ V(r,\Psi)\ r\ (r+e)\Big]\ dr \qquad (4.7)$$

where $(\dot{})$ denotes differentiation w.r.to Ψ .

Here, $\nu_\beta^2 = L + \omega_{\beta o}^2/\Omega^2$

$$L = 1 + \frac{3}{2}\frac{e}{\ell}$$

$$\omega_{\beta o}^2 = K_\beta / I_b$$

$$G = g S / I_b \Omega^2$$

$$V(r,\Psi) = \left[u(r,\Psi) + w(r,\Psi)\right]$$

In order to get the steady state solutions for the blade flapping motion one employs harmonic series representations for the disturbed inflow field and the blade pitch angle.

Let

$$V(r,\Psi) = V_0(r) + \sum_{n=1}^{\infty} V_n(r) \cos n\Psi$$
$$\beta(\Psi) = \beta_0 + \sum \beta_n \cos n(\Psi + \phi_n) \qquad (4.8)$$
$$\theta_p(r,\Psi) = \theta_0(r) + \sum \theta_n \cos n(\Psi + \phi_n')$$

One introduces equation (4.8) into equation (4.7) and takes the harmonic balance, while neglecting the coupling between the first harmonic excitation due to gravity and the higher harmonics of the flapping motion because this gravity effect is not appreciable for the model used in the experiment. The experimental wind

turbine model whose radius is relatively small rotates fast to keep the same tip speed ratio as the real wind turbine. Hence, the centrifugal force is so large that the gravity force is negligible, compared to this force. For real wind turbines, however, this does not generally hold true.

$$\beta_0 = \frac{LN}{2\nu_\beta^2}\left\{ \int_0^\ell \theta_0(r)\, r\,(r+e)^2\, dr + \int_0^\ell V_0(r)\, r\,(r+e)\, dr \right\} \qquad (4.9)$$

$$\beta_1 (\nu_\beta^2 - 1)\cos\phi_1 - G\beta_0 - M_{\dot\beta}\beta_1 \sin\phi_1 = \frac{LN}{2}\int_0^\ell r\left[(r+e)^2\theta_1 \cos\phi_1' + (r+e)\, V_1(r)\right] dr \qquad (4.10)$$

$$\beta_1(\nu_\beta^2-1)\sin\phi_1 + M_{\dot\beta}\beta_1\cos\phi_1 = \frac{LN}{2}\int_0^\ell r(r+e)^2\theta_1 \sin\phi_1'\, dr$$

$$\left\{(\nu_\beta^2-n^2)\cos n\phi_n - nM_{\dot\beta}\sin n\phi_n\right\}\beta_n = \frac{LN}{2}\left\{\int_0^\ell r(r+e)^2\, dr\,\theta_n \cos n\phi_n' + \int_0^\ell V_n(r)\,(r+e)\, r dr\right\}$$

$$\left\{(\nu_\beta^2 - n^2)\sin n\phi_n + nM_{\dot\beta}\cos n\phi_n\right\}\beta_n = \frac{LN}{2}\left\{\int_0^\ell r(r+e)^2 dr\,\theta_n \cdot \sin n\phi_n'\right\} \qquad (4.11)$$

When the blade pitch angle is kept constant, the coefficients of the flapping motion are obtained as follows.

$$\beta_1 = \frac{1}{\sqrt{(\nu_\beta-1)^2 + M_{\dot\beta}^2}}\left[G\beta_0 + \frac{LN}{2}\int_0^\ell r\, V_1(r)\,(r+e)\, dr\right] \qquad (4.12)$$

$$\beta_n = \frac{LN\int_0^\ell V_n(r)\, r\,(r+e)\, dr}{2\sqrt{(\nu_\beta^2 - n^2)^2 + n^2 M_{\dot\beta}^2}} \qquad n = 2, 3, \ldots . \qquad (4.13)$$

$$\text{Tan } n\phi_n = \frac{-n\, M_{\dot{\beta}}}{(\mu_\beta^2 - n^2)} \qquad n = 1, 2, 3, \ldots\ldots \quad (4.14)$$

Once the computed wake geometry is determined, the induced flow field in the rotor disk plane is computed. Then the coefficients of the inflow field series (V_n) are obtained by Fourier decomposition. From equations (4.9), (4.12) and (4.13) the coefficients of the rigid body flapping angle are calculated for the blade of constant chord and constant mass along the span. The flapping velocity is obtained from the time differentiation of the flapping angle (β). The effects of the blade flapping motion on the airloads are determined by simple superposition of the velocities due to the flapping motion and the inflow field. The equations for the blade flapping coefficients determines each harmonic of the flapping motion from the corresponding harmonic of the inflow field.

4.2 Pitch Angle Control to Minimize Flapping Moment Variations over a Rotation

The flow field on the wind turbine rotor disk plane is affected by the tower whether it is operating upwind or downwind of its tower. Thus the tower causes variations in the blade circulation and its flapping motion. However, the tower interference effects and hence the blade flapping motion, or the flapping moment variation can be reduced by controlling the blade pitch angle, enhancing the performance of the wind turbine at the same time. The coefficients ofthe pitch angle control (Θ_n) are determined from equations (4.10) and (4.11) by setting β_n equal zero.

$$\Theta_1 = \frac{-G\beta_o - \frac{LN}{2}\int_o^{\ell} r\,(r+e)\,V_1(r)\,dr}{\frac{LN}{2}\left[\frac{\ell^4}{4} + \frac{2}{3}\ell^3 e + \frac{1}{2}\ell^2 e^2\right]}, \qquad \phi_1' = 0 \qquad (4.15)$$

$$\Theta_n = \frac{-\int_o^{\ell} r\,(r+e)\,V_n(r)\,dr}{\left(\frac{\ell^4}{4} + \frac{2}{3}\ell^3 e + \frac{1}{2}\ell^2 e^2\right)}, \qquad \phi_n' = 0 \text{ for } n \geq 2 \qquad (4.16)$$

Also, from equation (4.11), the amount of the flapping motion control, or the control of the flapping moment variation by the unit pitch control is determined.

$$\frac{d\beta_n}{d\Theta_n} = \frac{LN\left[\frac{1}{4}\ell^4 + \frac{2}{3}\ell^3 e + \frac{1}{2}\ell^2 e^2\right]}{2\sqrt{(\nu_\beta^2 - n^2)^2 + n^2 M_{\dot\beta}^2}} \qquad n = 1, 2, \ldots\ldots (4.17)$$

Since the coefficients of the inflow field (V_n) as well as the induced velocities are dependent on the pitch control, equations (4.15) and (4.16) should be solved iteratively untill converged values of V_n and Θ_n are reached. For different Θ_n, the strength of the bound circulation varies and, also, the induced velocities on the rotor disk plane changes. These new induced velocities give the new Θ_n, according to equations (4.15) and (4.16). These equations show that the pitching variations should follow the inflow field variations, that is, there is no phase shift between the two.

4.3 Pitch Angle Control to Minimize Thrust Variations over a Rotation.

The unsteady blade lift acts on the tower as an unsteady exciting force while the wind turbine rotor is rotationg.

Obviously this kind of exciting force can cause some serious vibrational problems for the tower which undergoes strong side vibration. By controlling the blade pitch angle the variation of thrust generated by a blade can be minimized for a rotation of the blade. It would be better to minimize the thrust variation while keeping the blade flapping motion to a minimum than to accomplish only one of these two purposes. Referring to fig. 4.2, the elemental blade thrust is

$$dT = dL \cos\lambda + dD \sin\lambda$$

$$dL = \frac{1}{2}\rho U^2 a \alpha c \, dr$$

$$dD = \frac{1}{2}\rho U^2 C_d \, c \, dr$$

Hence, the thrust acting on one blade is

$$T = \frac{1}{2}\rho c \left[a\int U(\lambda + \theta)\Omega R^2 \eta d\eta + C_d \int U R^2 \Omega V \, d\eta \right]$$

Here $\lambda \cong \sin\lambda$, $U \cong \Omega R \eta$

$$\frac{T}{\rho \pi \Omega^2 R^4} = L_T = \frac{\sigma}{2b}\left[a\int (V\eta + \theta_p \eta^2) \, d\eta + C_d \int V\eta \, d\eta \right] \qquad (4.18)$$

The coefficients of the required pitch angle control are obtained by employing series representations for the thrust and for the inflow field and by taking the harmonic balance of the resulting equation.

Let

$$L_T = L_{T0} + \sum L_{Tn} \cos n (\Psi + \phi_n)$$

$$V(\eta, \Psi) = V_0(\eta) + \sum_n V_n(\eta) \cos n\Psi$$

$$\theta_p(\Psi) = \theta_0(\eta) + \sum \theta_n \cos n (\Psi + \phi_n')$$

Then, equation (4.18) is decomposed as follows.

$$L_{T0} = \frac{\sigma}{2b}\left[a\int_{\eta_{rc}}^{1}\{V_0(\eta)\eta + \theta_0(\eta)\eta^2\}d\eta + C_d\int_{\eta_{rc}}^{1} V_0(\eta)\eta\, d\eta\right] \quad (4.19)$$

$$\left.\begin{aligned} L_{Tn}\cos n\phi_n &= \frac{\sigma}{2b}\left[(a + C_d)\int_{\eta_{rc}}^{1} V_n(\eta)\eta\, d\eta \right.\\ &\quad \left. + a\,\theta_n \cos n\phi_n' \int_{\eta_{rc}}^{1} \eta^2 d\eta\right] \\ -L_{Tn}\sin n\phi_n &= \frac{\sigma}{2b}\left[-a\,\theta_n \sin n\phi_n' \int_{\eta_{rc}}^{1} \eta^2 d\eta\right] \end{aligned}\right\} \quad (4.20)$$

Again, the coefficients of the pitch angle control (θ_n) are obtained by setting L_{Tn} to be zero.

$$\theta_n = -\frac{3(1 + C_d/a)}{(1 - \eta_{rc}^3)}\int_{\eta_{rc}}^{1} \eta V_n(\eta)\, d\eta, \quad \phi_n' = 0 \quad (4.21)$$

Furtheremore, the sensivity of the blade thrust to pitch change, or the amount of the thrust control by the unit pitch control is obtained from equation (4.20).

$$\frac{dL_{Tn}}{d\theta_n} = \frac{\sigma a}{2b}\int_{\eta_{rc}}^{1}\eta^2 d\eta = \frac{\sigma a}{6b}(1 - \eta_{rc}^3) \quad (4.22)$$

As mentioned in setion 4.2, the coefficients (V_n) are dependent on the blade pitch angle θ_n. Therefore, the required pitch control

angle should be determined iteratively from equation (4.21) in the same manner which was used to determine the Θ_n which minimize the blade flapping motion. The equation (4.21) shows that there is no phase shift between the pitching variations required to minimize the thrust variations and the inflow field variations.

SECTION 5

RESULTS AND COMPARISON WITH EXPERIMENT

5.1 Steady Results

The calculated power coefficients in a uniform flow for pitch angles of 0° and 4° are presented in fig. 5.2 with measured results from [13]. The thrust coefficients are shown in fig. 5.3. The drag representation, $C_d = 0.01 + 1.5 \cdot \alpha^2$, is used. The results shown are in good agreement with experiement for tip speed ratios where stall effects are not important. The same stall model as used in [7] is employed with stall angle, 0.2 radians. Fig. 5.2 suggests that this stall model does not describe the stall history adequately.

In fig.5.4 to fig.5.7 the calculated power and thrust coefficients are compared with experiments and some results from [7].The same semi-rigid wake model as the one used in [7] is employed in these calculations. Here the induced velocity on the rootcut or the blade tip is taken to be half of the induced velocity at the inboard control point of the blade. For an 8° pitch angle the three results give almost identical values of thrust and power coefficients. The departure of the theoretical predictions from the experimental results seems to show that for an 8° pitch angle the wake behaves like the new wake model used in calculating the results in fig.5.2 and fig.5.3 which includes the retardation and radial movement of the vortices in the first spiral. It is obvious from fig.5.4 to fig.5.7 that the present analysis give better results than those

obtained in [7].

In the present analysis 15 control points are chosen, which means that 15 coefficients of the bound circulation series are computed. As the number of harmonics is increased, the magnitude of the corresponding harmonic coefficient decreases rapidly as shown in fig. 5.8. For every calculation the coefficients for the 7 th and higher harmonics are negligible. The first and second coefficients are especially dominant. Ten control points and harmonics are thought to be adequate to obtain pratical results. All the calculations in the present analysis converge within three iterations.

The bound circulation distributions along the blade are shown for two pitch angles in fig. 5.9. It shows that the bound circulation increases near the root and decreases near the tip as the blade pitch angle increases. At the tip $d\Gamma/d\eta$ is infinite in both cases. It is because $d\Gamma/d\theta$ is finite at the tip and hence $d\Gamma/d\eta = 2\frac{d\Gamma}{d\theta}\cdot\frac{1}{\sin\theta}$ $= \infty$ for $\theta = 0$ or π . Induced velocities along the span are presented in fig. 5.10 with the induced velocities on the root cut or the blade tip. It is interesting to notice in the case of 4° pitch that the induced velocities are almost constant and about 1/3 of the free stream velocity which the momentum theory predicts to be the ideal condition for maximum power. The induced velocity on the blade tip is shown to be less than half of the velocities induced inside of that point.

The dependence of the induced velocity at the blade tip on the radial distance, d, is presented in fig. 5.11. As d approaches zero, the induced velocity approaches infinity. The converged value occurring for $d > 0.03$ was used in calculations.

5.2 Shear Flow

Calculated disturbance pressure ratios are presented in fig. 5.12 with experimental results from [13] and the calculated results with the semi-rigid wake from [7]. They are in excellent agreement with experiment, and the effect of the shed wake has increased when wake was allowed to become non-rigid. This is due to the fact that the seperation of the shed vortex lines from the rolled-up vortices position them nearer the rotor disk plane than in the previous semi-rigid wake model. Fig. 5.12 shows this phenomena clearly. For powered rotors the shed vortex lines will be located below the rolled-up vortices and hence their effects on unsteady airloads will be decreased. It is demonstrated from fig. 5.12 that the seperation of the shed wake surface from the plane determined by the rolled-up vortices are desirable, especially for the prediction of unsteady airloads and the approach used in the present calculations works.

Tower reflection effect is inherently included in the experimental results of fig. 5.12. The calculated disturbance pressure ratios are obtained by using the equivalent shear flow without the tower reflection effect. In fig. 5.13 the result for shear flow with tower reflection is compared with the one for the equivalent shear flow without the tower reflection. As far as the disturbance pressure ratio is concerned, the two results give the same value.

But shear flow with equivalent slope as tower reflection is a little optimistic in the prediction of the performance coefficients as indicated by the respective values of C_p in fig. 5.13.

5.3 Tower Effects

The calculated airloads at the 75% spanwise position of the blade are presented in fig. 5.14 for the rotor model operating upwind of the tower in steady,uniform flow. For the free stream velocity reduction (VR), 0.1165 is used and the value 0.375 non-dimensioned by the rotor radius is used for the width (ζ) of the flow field interfered by the tower in the calculations. These two values were obtained from the experimental wind profile as shown in fig. 5.15. The computed unsteady airloads, which are nomalized by the average, are shown in fig. 5.16 with experimental values for the tower reflection case with Xmas tree shown in fig. 5.1. From the free stream velocities measured at 75 % spanwise position of the blade, the equation to give the wind profile on the rotor disk plane is derived. The velocities computed from this equation are shown in fig. 5.15 with the measured velocities. The instaneous thrust and performance coefficients are presented in fig. 5.17 for the tower reflection with Xmas tree. They are periodic by 180° because the rotor has two blades. C_p varies more than 50 % of its maximum along the azimuthal angle. This means that the torque acting on the wind turbine shaft varies periodically by that much. C_T variations are within 30 % of its maximum, and hence a vibratory force of this order acts on the tower . The predicted unsteady

disturbance airload ratios are in close agreement with experimental values for the tower reflection, even for the flow disturbed due to Xmas tree. The variations in airloads on the blade show the same form variations as the free stream velocities on the rotor disk plane.

Wind profile equation (3.7) gives results in good agreement with experimental values behind the tower as shown in fig 5.18. That equation is, thus, believed to be the proper characterization of the wind profile behind the tower. The calculated peak disturbance pressure ratio is shown to be slightly larger than the measured value in fig. 5.19. Also, fig. 5.19 shows that it reduces the peak airload deficit drastically.

It is shown in fig. 5.20 that the use of the non-rigid wake model has increased the induced velocities on the blade and hence has reduced the airloads on the blade, compared to the semi-rigid wake model. Reductions are 10 % in airloads, 13 % in C_p and 7 % in C_T. The seperation of the shed vortex sheet from the plane defined by the rolled-up tip or root vortices has increased the effect of the shed wake, that is, has reduced the peak airload variation by 4 %.

5.4 Effect of Blade Motion on Airloads

The rigid body flapping velocity shown in fig. 5.21 is less than 2 % of the free stream velocity. The blade angle of attack or the airloads will be changed by this percentage. Therefore, the effect of the flapping velocity on airloads are negligible for this model wind turbine rotor used in the experiments. This conclusion

does not imply that it is true for any wind turbine rotor because the structural design of the blade can be varied pretty much from this experimental model. Generally, it is believed that the one per revolution excitation due to the tower is not enough to cause fast blade flapping motion, except the resonance case. It is shown in fig. 5.21 that the maximum flapping angle is about 0.4° for this model. The deflection of the blade tip due to this flapping angle is 4 % of the blade chord. The nearest distance between the following blade and the tip vortex from the preceding blade is farther than one chord length at least. Also, the tip vortex is located outside the blade tip because the tip vortex expands fast in the first spiral. Therefore, this flapping angle will not have apprecable effect on airloads. When the deflection of the tip exceeds half chord length, it is believed that the deflection of the blade due to flapping motion should be included in determining the relative distance between the blade and the tip vortex.

The computed inflow velocity is compared with the one calculated from the 10 harmonics of the corresponding Fourier series in fig. 5.22. That figure shows that the 10 terms of the Fourier series still do not describe the peak velocity variation. It seems that some caution should be paid for using the Fourier series for the representation of the inflow field.

SECTION 6

DISCUSSION AND CONCLUSIONS

6.1 Discussion

For the transport velocity of the tip vortex, instead of using one constant velocity for the tip vortex in the first blade spacing and a different constant velocity outside the first blade spacing as in [4] and [5], varying velocities are used for the first spiral of tip vortex. This was done because the velocities induced by the first spiral tip vortex are of almost the same order as those induced by the near wake. The assumption that the induced velocity on the tip or root vortex varies linearly until it is doubled at the first blade encounter is open to question. But it is not likely that the induced velocity on the tip vortex is suddenly doubled. Experimental investigation on the wake geometry or the free wake analysis can give information about how the induced velocity on the tip vortex varies. The non-rigid wake model used for the non-uniform flow shows that the induced velocity varies continuously rather than is doubled suddenly. The accurate calculation of the induced velocity on the tip vortex in the first spiral is required in view the fact that the correct axial and radial positioning of that vortex is important for the good prediction of airloads and performance. All these facts necessitate the theory which can handle the transient rolling process of trailing vortices and the effect of the tip shape or its modification on the rolling. Obviously the flow field near the blade tip is very complex and three dimensional. That theory can give the way to attenuate the concentrated vortex,

hence to increase the performance. The circulation distribution of the rolled-up vortex only rather than the transient one can be related to the load distribution of the wing for the non-rotating wing.

The rate of convergence becomes much slower with the non-rigid wake model than with the usual semi-rigid wake model because the wake undergoes considerable deformation and the geometry varies considerably per iteration in the former than in the latter case. The induced velocities by the far wake are approximately doubled near the blade tip when the non-rigid wake model is used, compared to the results obtained when the usual semi-rigid wake model is used in [7].

The retardation of the tip vortex places the tip vortex so close to the rotor blade that it causes a significant increase in the induced velocities near the blade tip, which results in a reduction of the wind turbine performance. This retardation has the effect on the wind turbine performance which has the reverse tendency as that of the rapid contraction of the rotor slip stream in the hovering flight of a helicopter noticed in ref. [4]. This contraction makes the tip vortex pass inside the blade tip and this vortex passage increases the angle of attack near the tip for the powered rotor.

It is interesting to note that $d\beta_n/d\theta_n$ does not depend on the flow condition on the rotor disk plane and is determined by the initial blade design. For the wind turbine of fig. 5.1, $d\beta_1/d\theta_1 = 0.3$ and $dL_{T1}/d\theta_1 = 0.1$.

6.2 Conclusions

Lifting line theory using a sine series representation of bound circulation with new wake geometry gives pratical results and is very cost effective. With a more realistic wake geometry lifting line theory will acurately predict the experimental values. A further conclusion is that the discrepancy between experiment and theory in [7] is due to use of the approximate wake geometry, especially due to the neglect of the retardation and radial movement of the tip vortex. It is believed that the scheme developed to compute the initial induced velocity on the tip or the root vortex is useful and reliable, and that the vortices trailed from the tip or root become the center of the rolled-up vortices as long as $d\Gamma/d\eta$ has its largest value at that point .

It is recommended that the research to find the theory to handle the transient rolling process be done with the experimental survey of that phenomena. This suggestion implies that such a kind of research can reward its cost by opening the way to solve many problems related to strong tip vortex.

It is recommended that the shed line vortices in the far wake be located on a plane other than the one defined by the rolled-up tip and root line vortices.

The main effect of the tower has been found to be a reduction in airloads on the blades with almost the same form as that of the tower effect on velocity. It is concluded that the vertical transport velocities of the tip vortices change rapidly in the first

spiral in the wake, which invalidates the assumption that vortices retain the relative velocities of the flow passing through the rotor.

It is concluded that the disturbance pressure ratio can be accurately calculated by using the equivalent shear flow for the case of shear flow which includes tower reflection effect and that the shed wake can not be neglected in calculating the disturbance airload for the tower shadow case. Further conclusion is that the non-rigid wake model, which is developed by systematic modifications of semi-rigid wake, is accurate and fairly simple, compared to free wake model.

References

1. Miller, R.H. "Unsteady Air Loads on Helicopter Rotor Blades". Royal Aeronautical Society Journal, Vol.68,No.640, April 1964.

2. Miller, R.H. "On the Computation of Airloads Acting on Rotor Blades in Forward Flight". American Helicopter Society Journal , Vol. 7, No.2, April 1962.

3. Miller, R.H. "Rotor Blade Harmonic Air Loading". AIAA Journal , Vol.2, No.7, July 1964.

4. Jenney, D.S., Olson, J.R., and Landgrebe, A.J. "A Reassessment of Rotor Hovering Performance Prediction Methods". American Helicopter Society Journal, Vol.13, No.2, April 1968.

5. Landgrebe, A.J. and Egolf, T.A. "Rotorcraft Wake Analysis for the Prediction of Induced Velocities". United Technologies Research Center; USAAMRDL Tech. Rpt.75-45,Eustis Directorate, U.S. Army Mobility R&D Lab, Fort Eustis, Virginia, January 1976.

6. Scully, M.P. "Computation of Helicopter Wake Geometry and Its Influence on Rotor Harmonic Airloads". Massachusetts Institute of Technology,Ph.D. Thesis, February 1975.

7. Thomas, H.M., Chung, S.Y., and Gohard, J.C. "Steady and Unsteady Aerodynamics". Chapter III, Wind Energy Conversion, Final Report, NSF Grant No.AER 75-00826, Oct. 1976.

8. DeJarnette, F.R., "Arrangement of Vortex Lattices on Subsonic Wings". Vortex Lattice Utilization, NASA SP-405,May 17-18,1976.

9. Sullivan, J.P. "The Effect of Blade Sweep on Propeller Performance". AIAA Paper No. 77-716,AIAA 10th Fluid & Plasma Dynamics Conference, Albuquer, N.Mex./June 27-29, 1977.

10. Landgrebe, A.J., Moffitt, R.C., and Clark, D.R. "Aerodynamic Technology for Advanced Rotorcraft- Part I". J. American Helicopter Society, Vol.22, No.2, April 1977, pp. 21-27.

11. Kocurek, J.D. and Tangler, J.L. "A Prescribed Wake Lifting Surface Hover Performance Analysis". 32nd Annual National Forum ,American Helicopter Society,Washington, D.C.,May 1976.

12. Miller, R.H. and Martinez-Sanchez,M. "Wind Turbine Performance". Chapter II, Wind Energy Conversion, Final Report, Oct.1976.

13. Dugundji, J. and Larrabee, E.E. "Experimental Investigation". Chapter VII, Wind Energy Conversion, Final Report, Oct.1976.

14. Clark,David R. and Reiper,Albert C. "The Free Wake Analysis-A Method for the Prediction of Helicopter Rotor Hovering Performance". American Helicopter Society Journal, Vol.15, NO.1, January 1970.

15. Batchelor, G.K.,An Introduction to Fluid Dynamics, Cambridge at the University Press, 1967.

TABLE I

ROTOR MODEL USED IN THE ANALYSIS

$\sigma = 0.1061$

$C_d = 0.01 + 1.5 \cdot \alpha^2$

2 Blades

No Twist

No Taper

$\eta_{rc} = 0.2$

TABLE II

MODELING OF THE PROBLEM

	Steady Program	Unsteady Program
No. of Wake Spirals Used in Calculations	10.5	10
No. of Control Points	15	6
Near Wake Region	$\Psi = 0 - 10^\circ$	$\Psi = 0 - 15^\circ$
Intermediate Wake Region	$10^\circ - 90^\circ$	$15^\circ - 90^\circ$
Far Wake Region	$90^\circ -$ 10.5 spirals	$90^\circ -$ 10 spirals
Wake Azimuthal Increment	X	15
Tip or Root Vortex Elements	constant strength varying directions	varying strengths " directions
Azimuthal Integration Interval of Line Vortex		
(1) Element in Near Wake	10°	5°
(2) " in Intermediate Wake	10°	15°
(3) " in Far Wake	20°	15°

TABLE III

PROFILE DRAG REPRESENTATION EFFECT

Advance ratio $\mu = 0.1197$, Pitch angle $\Theta_p = 4^\circ$

Profile Drag Representation C_d	Shed Wake Neglected		Shed Wake Included	
	C_p	C_T	C_p	C_T
$0.01 + 0.5 \cdot \alpha^2$	0.123	0.333	0.121	0.331
$0.01 + 1.5 \cdot \alpha^2$	0.109	0.333	0.107	0.331

* Rotor is operating upwind of the tower in uniform flow.

TABLE IV

SHED WAKE EFFECTS

μ	Shed Wake	C_p	C_T	$\Delta\Gamma_b/\Gamma_{AV}$
0.18	IN(included)	0.178	0.363	0.169
	NE(neglected)	0.178	0.362	0.201
0.1197	IN	0.136	0.368	0.207
	NE	0.136	0.367	0.314
0.0972	IN	0.055	0.331	0.318
	NE	0.055	0.330	0.462
0.1087	IN	0.107	0.359	0.230

* Rotor is operating in shear flow with pitch angle $\Theta_p = 4^\circ$

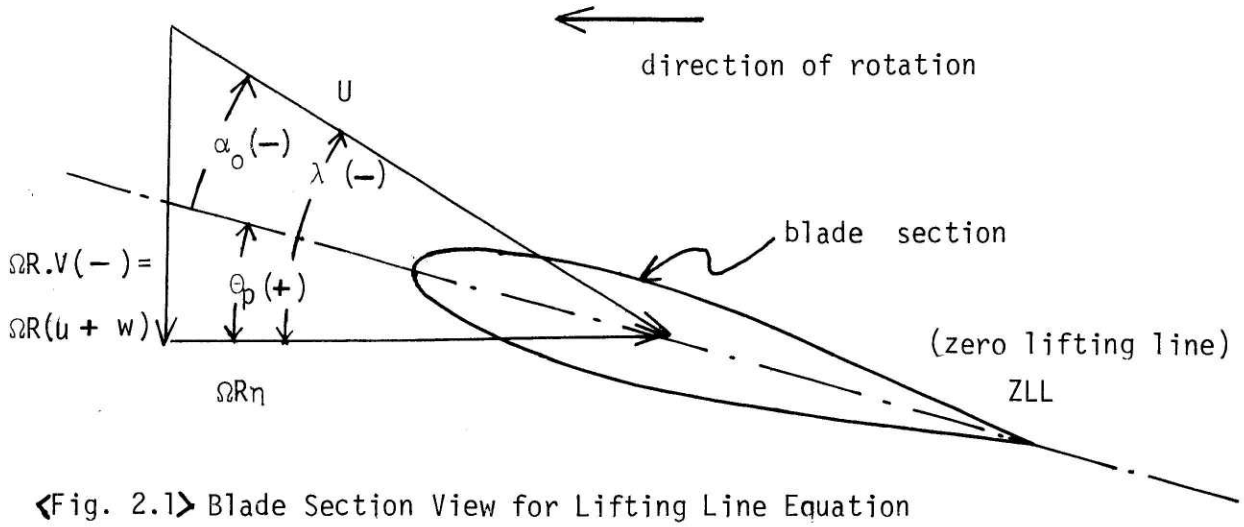

<Fig. 2.1> Blade Section View for Lifting Line Equation

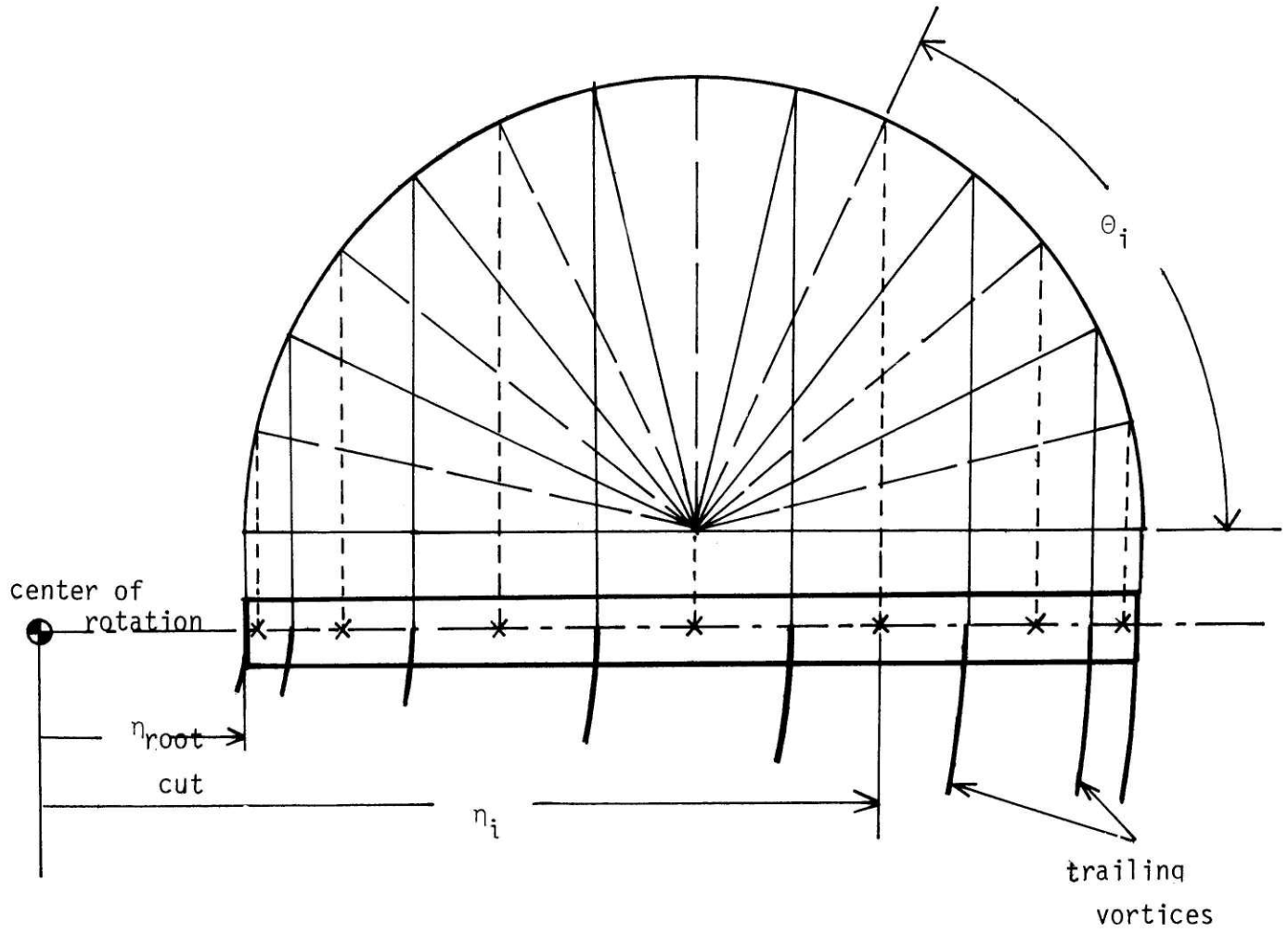

<Fig. 2.2> Arrangement of Trailing Vortices

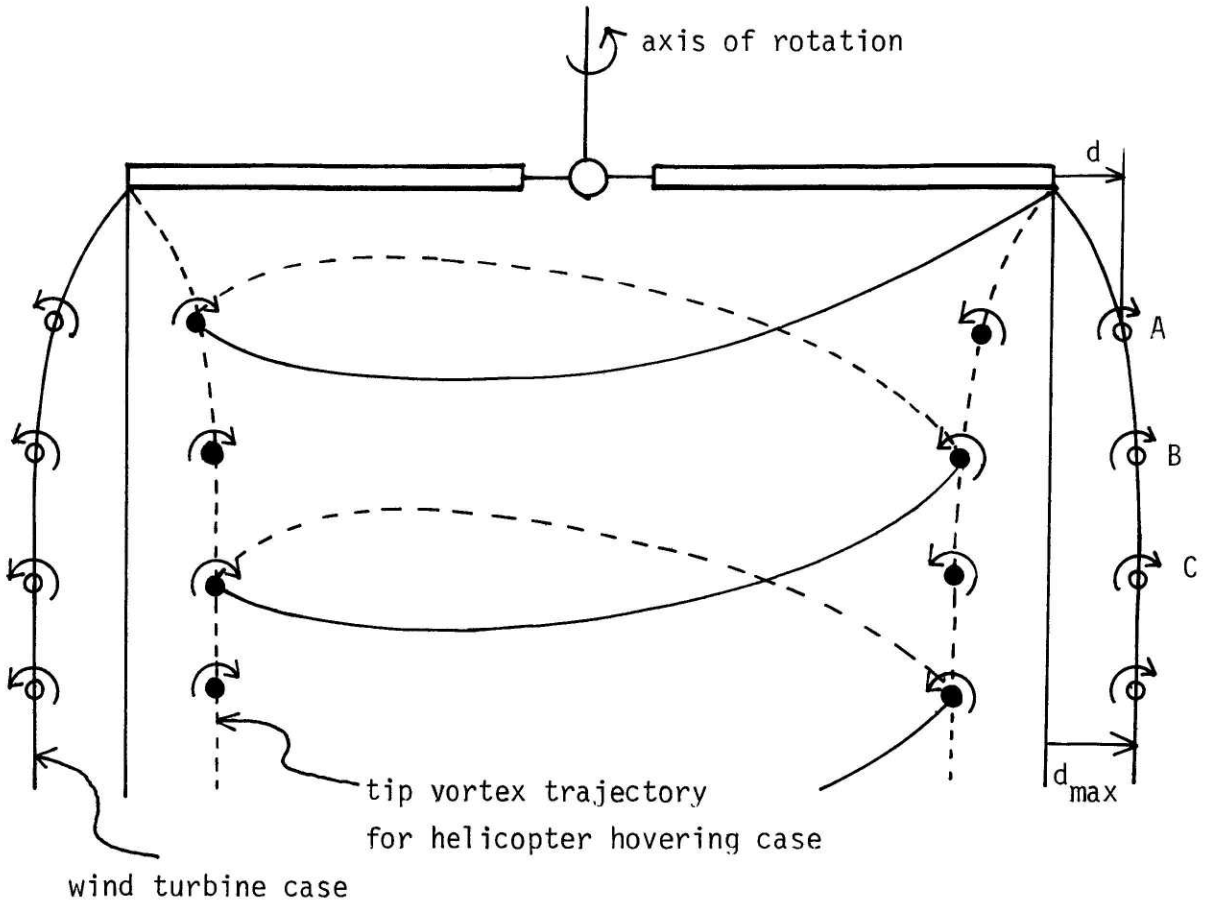

<Fig. 2.3> Tip Vortex Radial Movement Trajectory

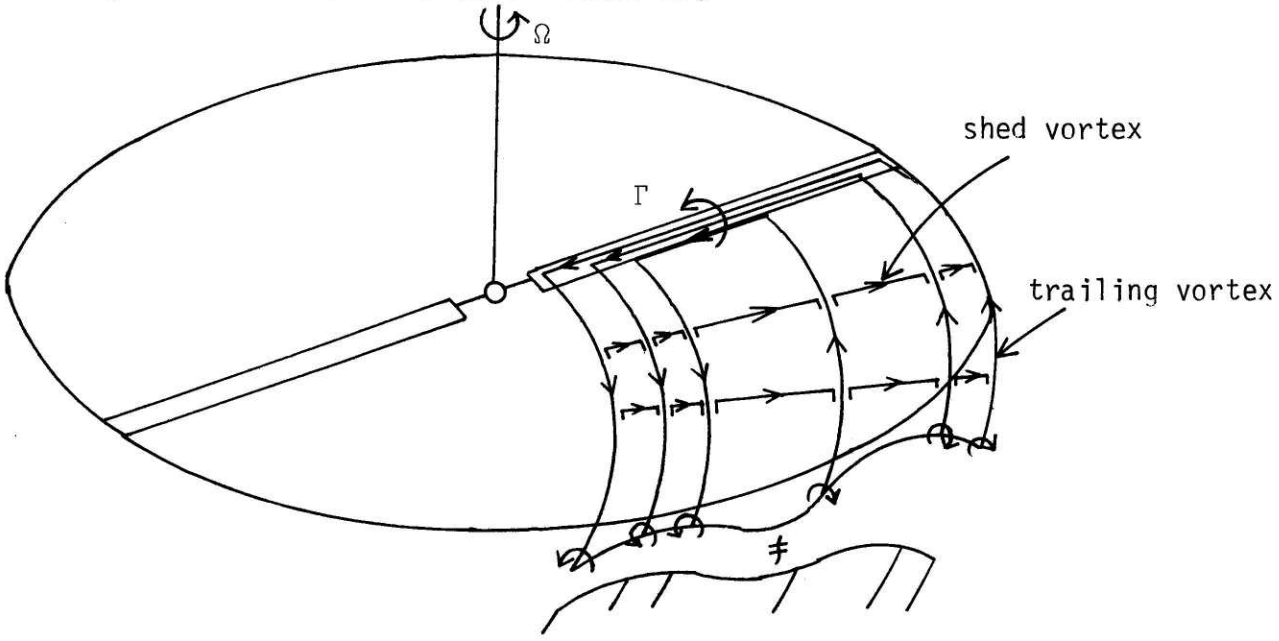

<Fig. 3.1> Trailing and Shed Vortex System

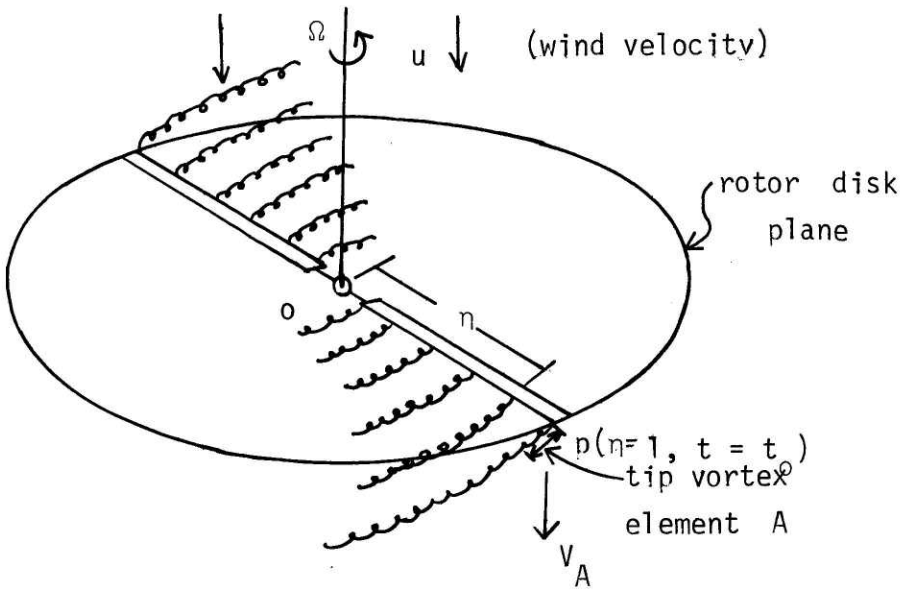

<Fig. 3.2A> Representation Of Transport Velocity of Tip Vortex at $t=t_o$

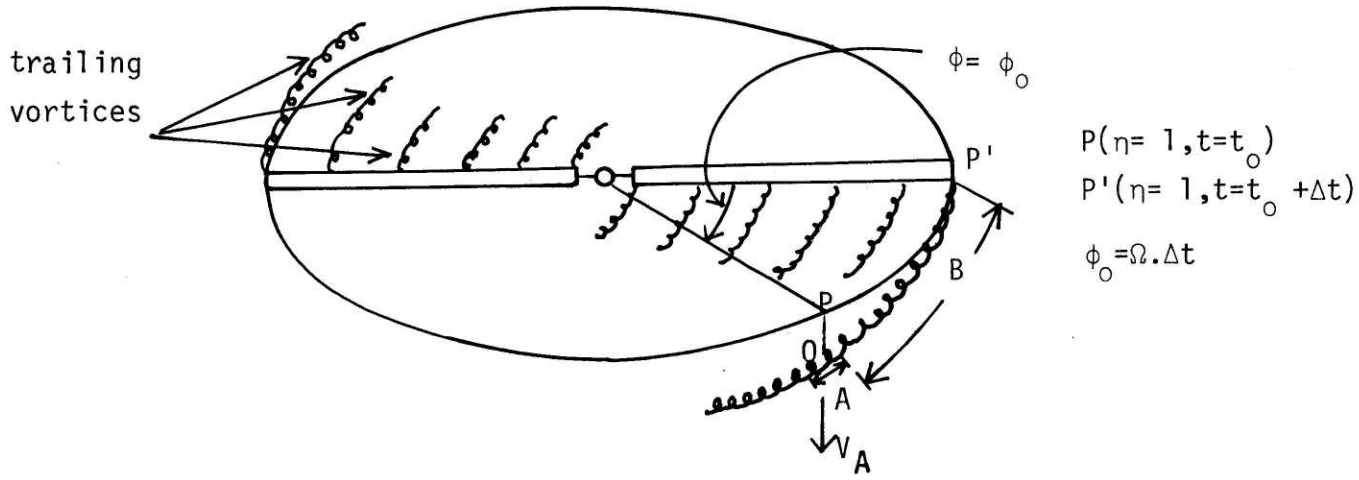

<Fig. 3.2B> Transport Velocity of Tip Vortex at $t = t_o + \Delta t$

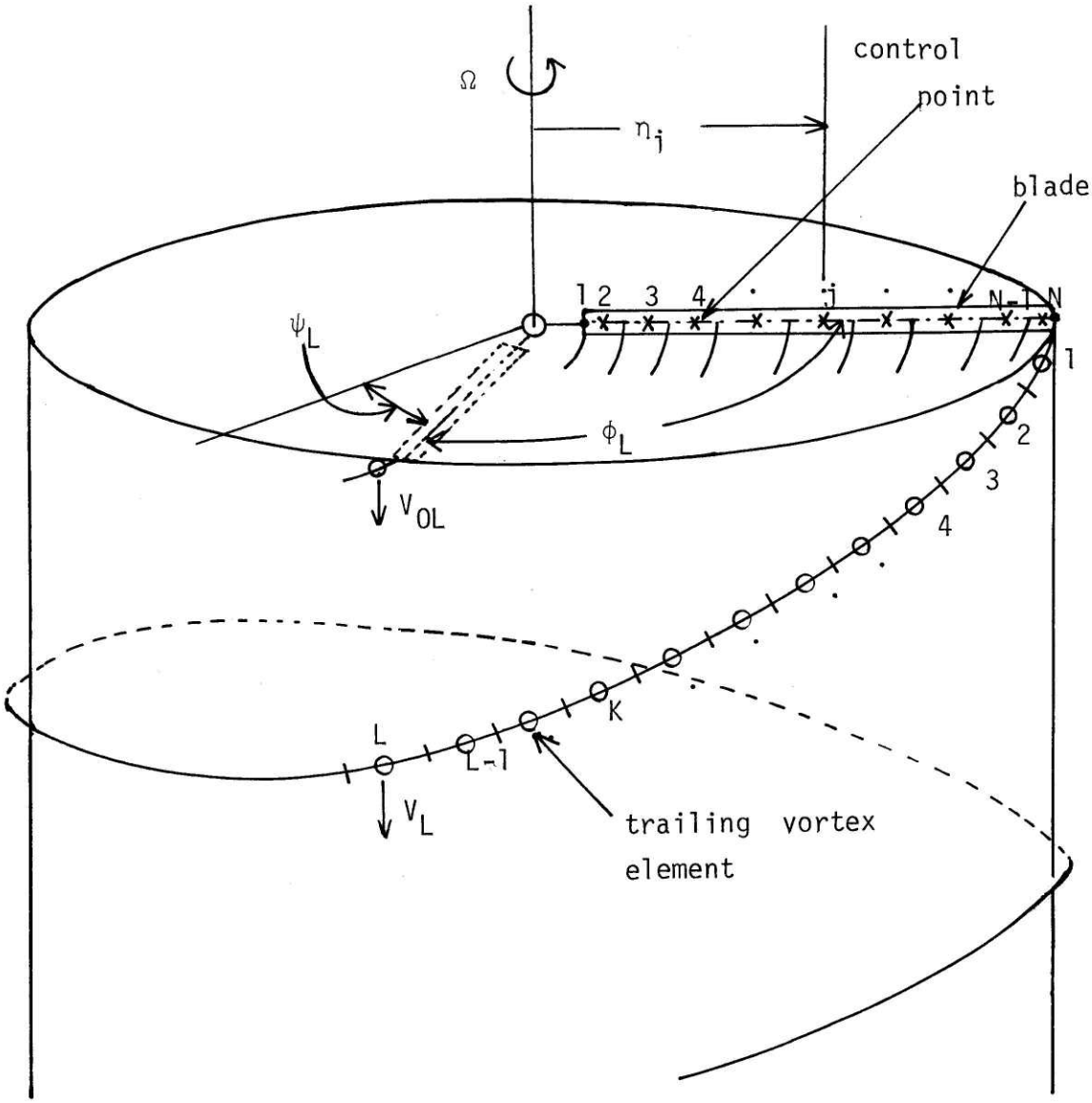

<Fig. 3.3>Illustration for the Calculation of Nonlinear Movement of Tip Vortex

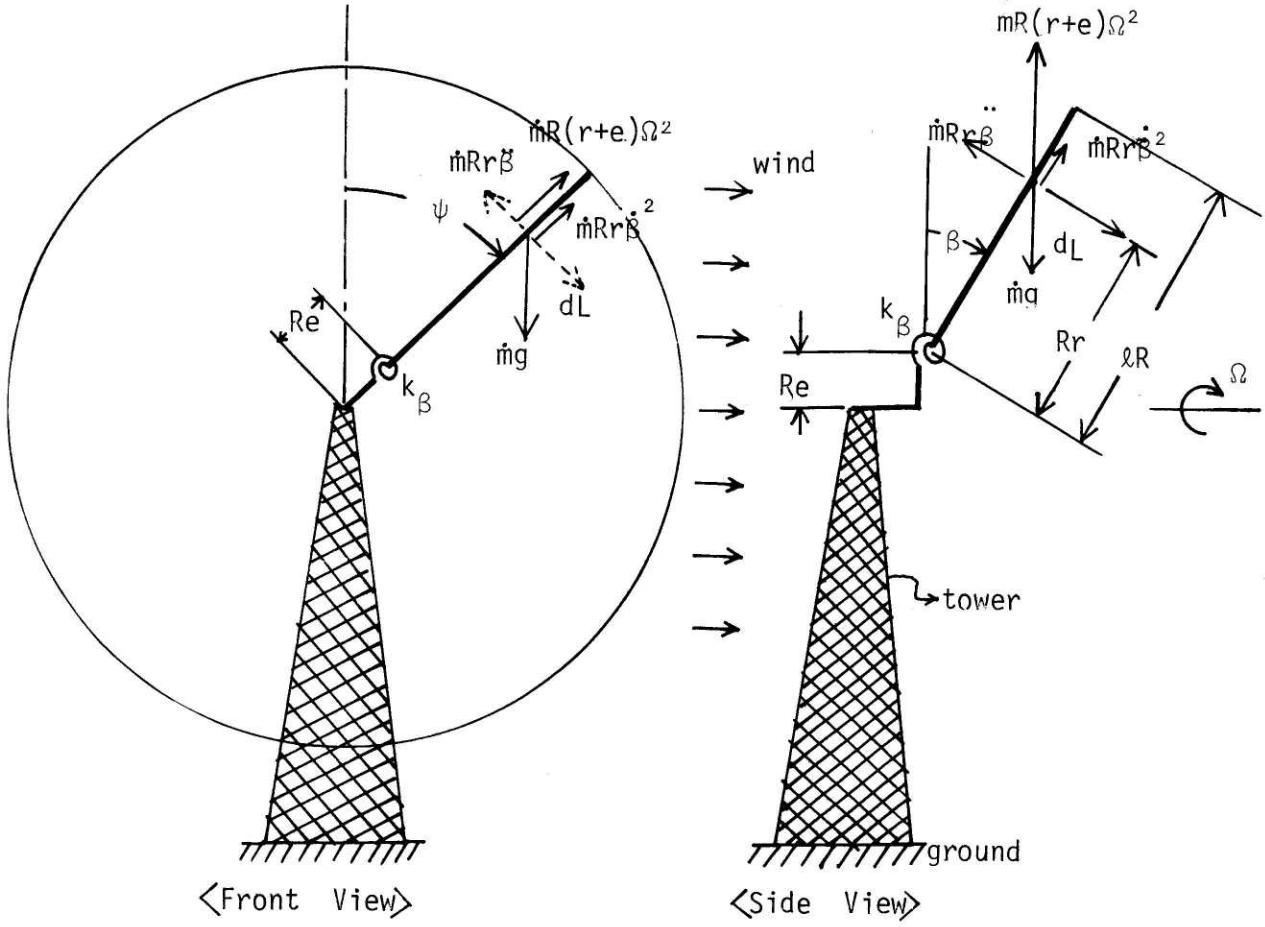

<Fig. 4.1> Forces Acting on the Blade Including Inertia Forces

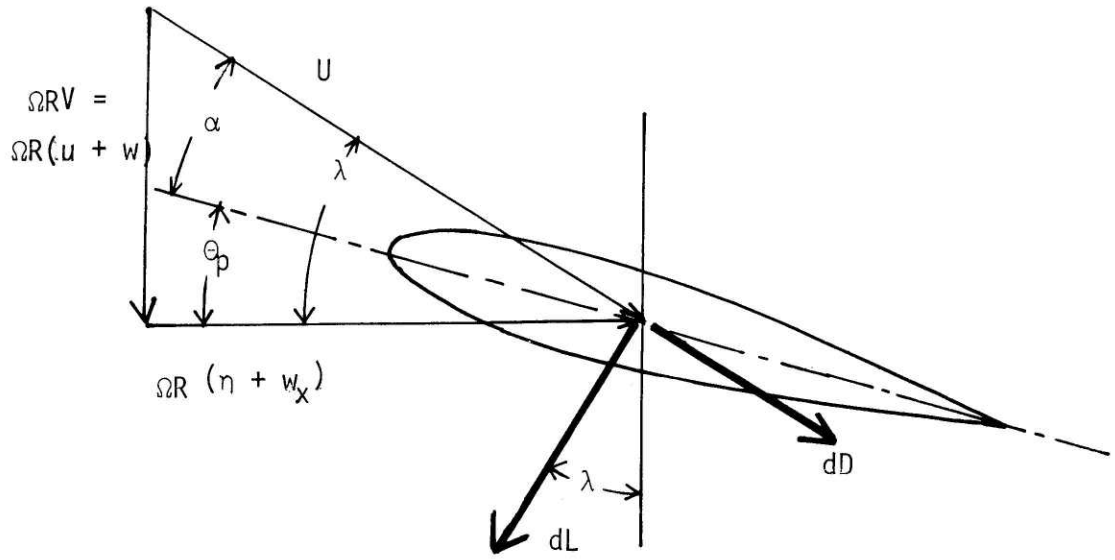

<Fig. 4.2> Flow around Blade Element

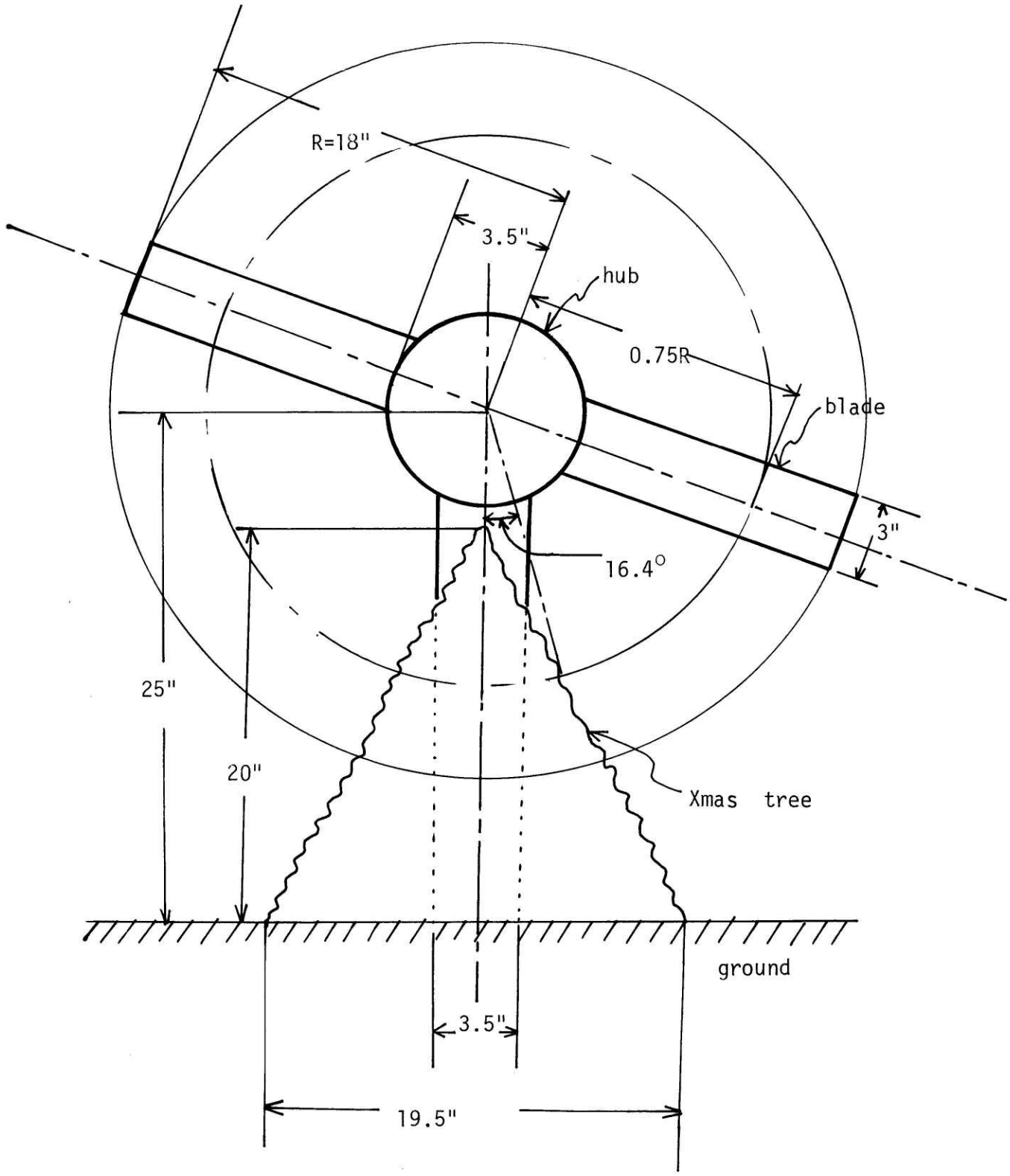

<Fig. 5.1> Front View of the Tower and the Wind Turbine Rotor with Xmas Tree (used in Experiment)

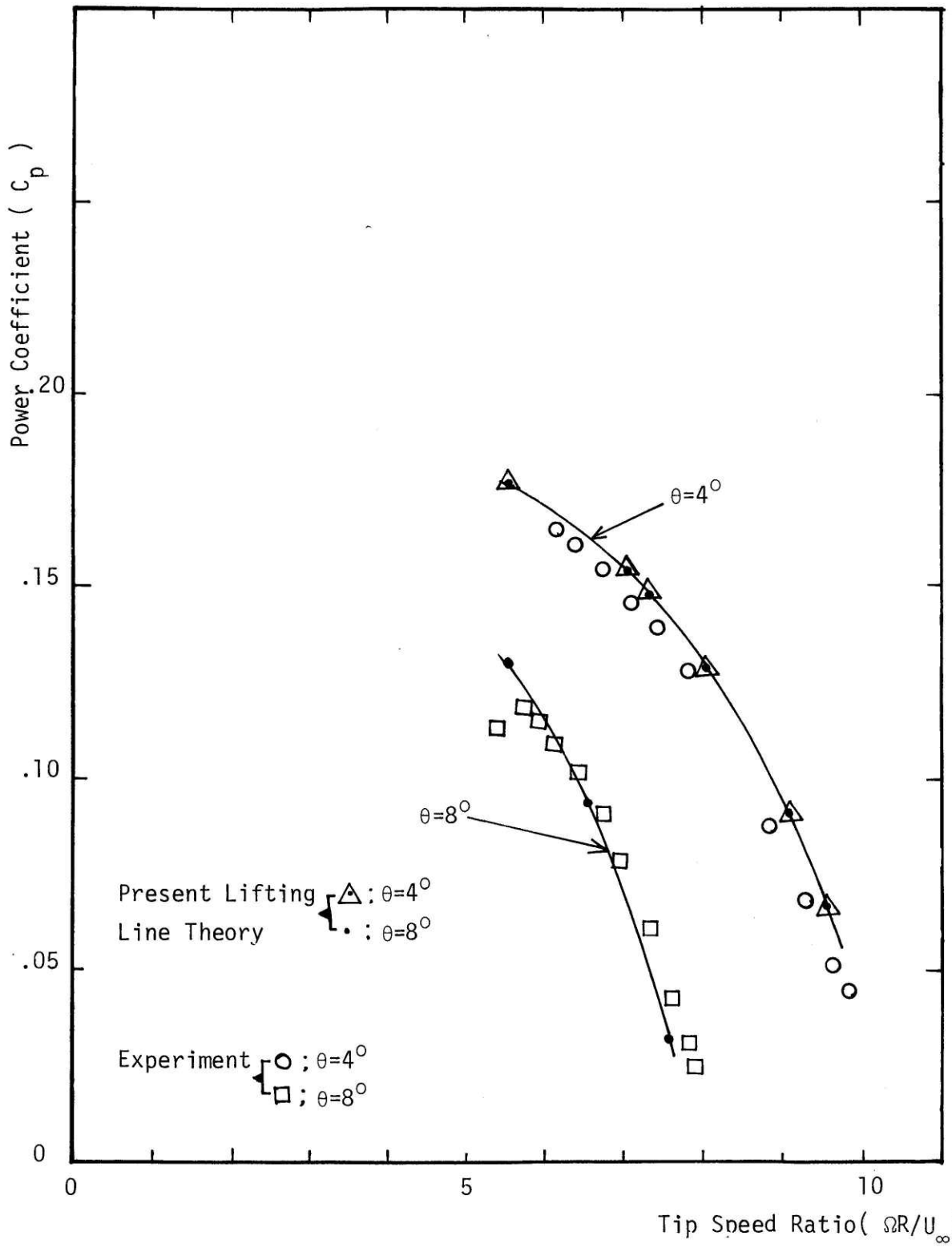

<Fig.5.2>Comparison of Present Lifting Line Theory and Experiment

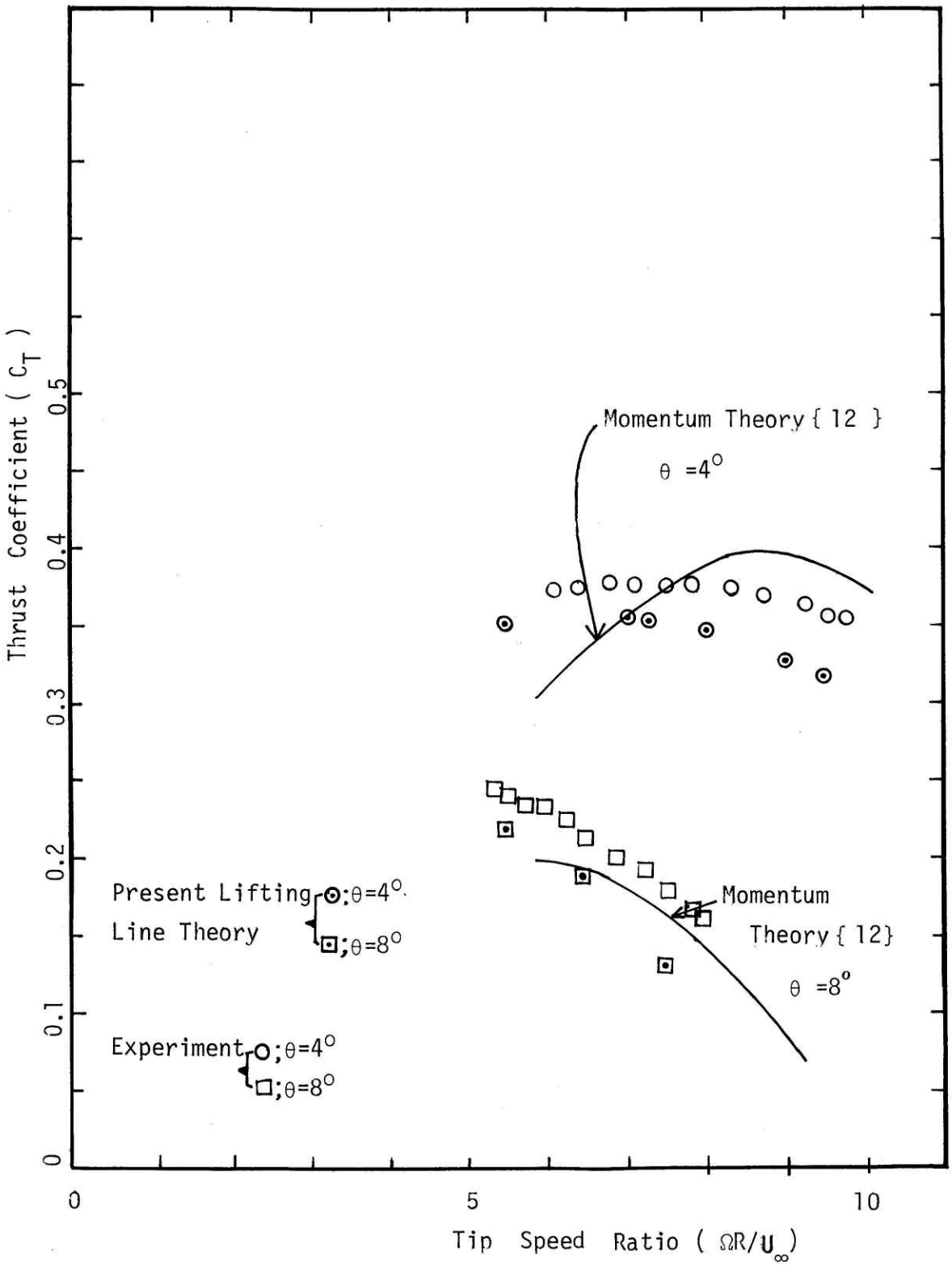

<Fig. 5.3> Comparison of Lifting Line Theory, Momentum Theory, and Experiment

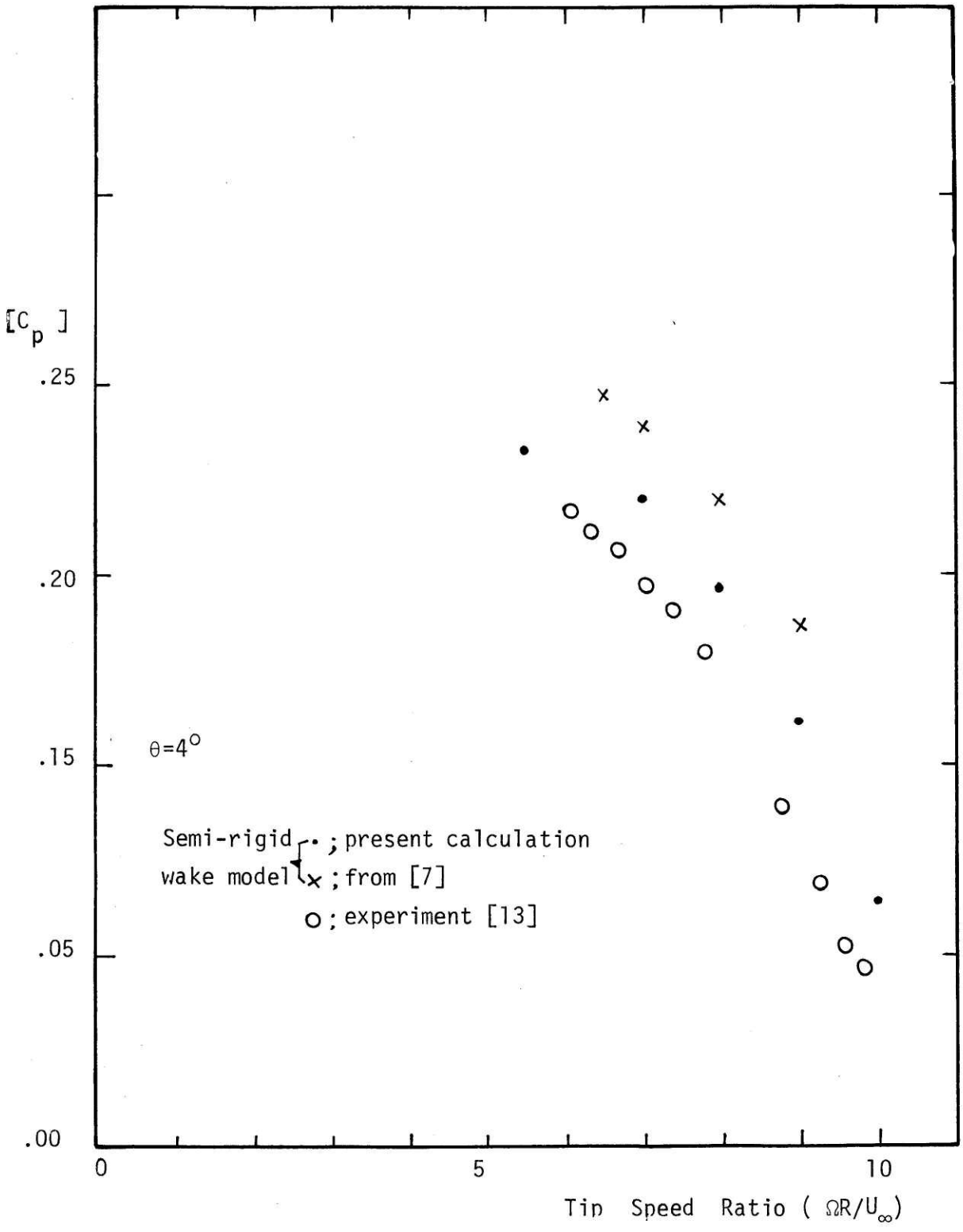

<Fig.5.4>Comparison of Present Lifting Theory and the Previous one [7]

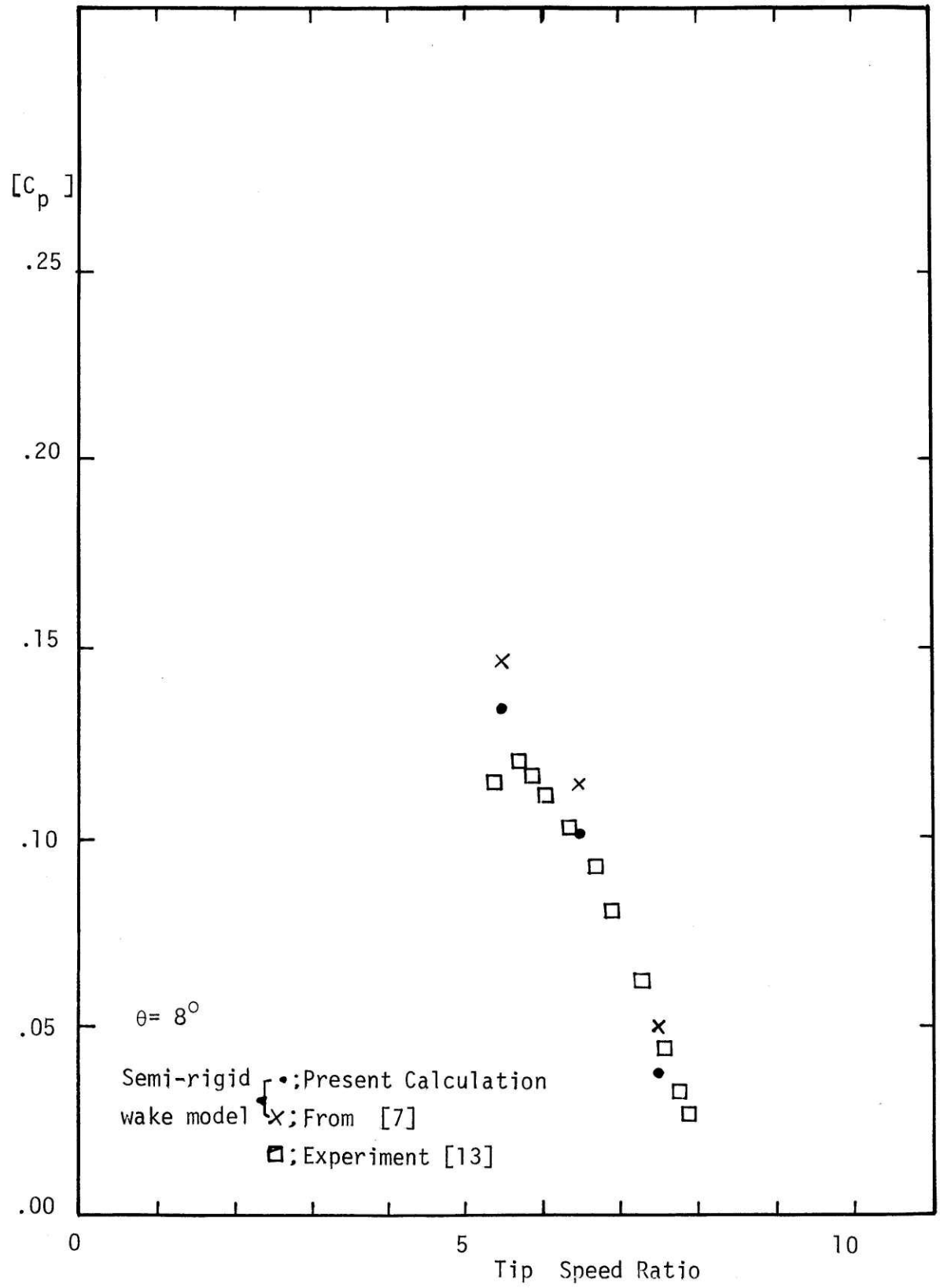

<Fig. 5.5> Comparison of Present Lifting Line Theory and Previous One

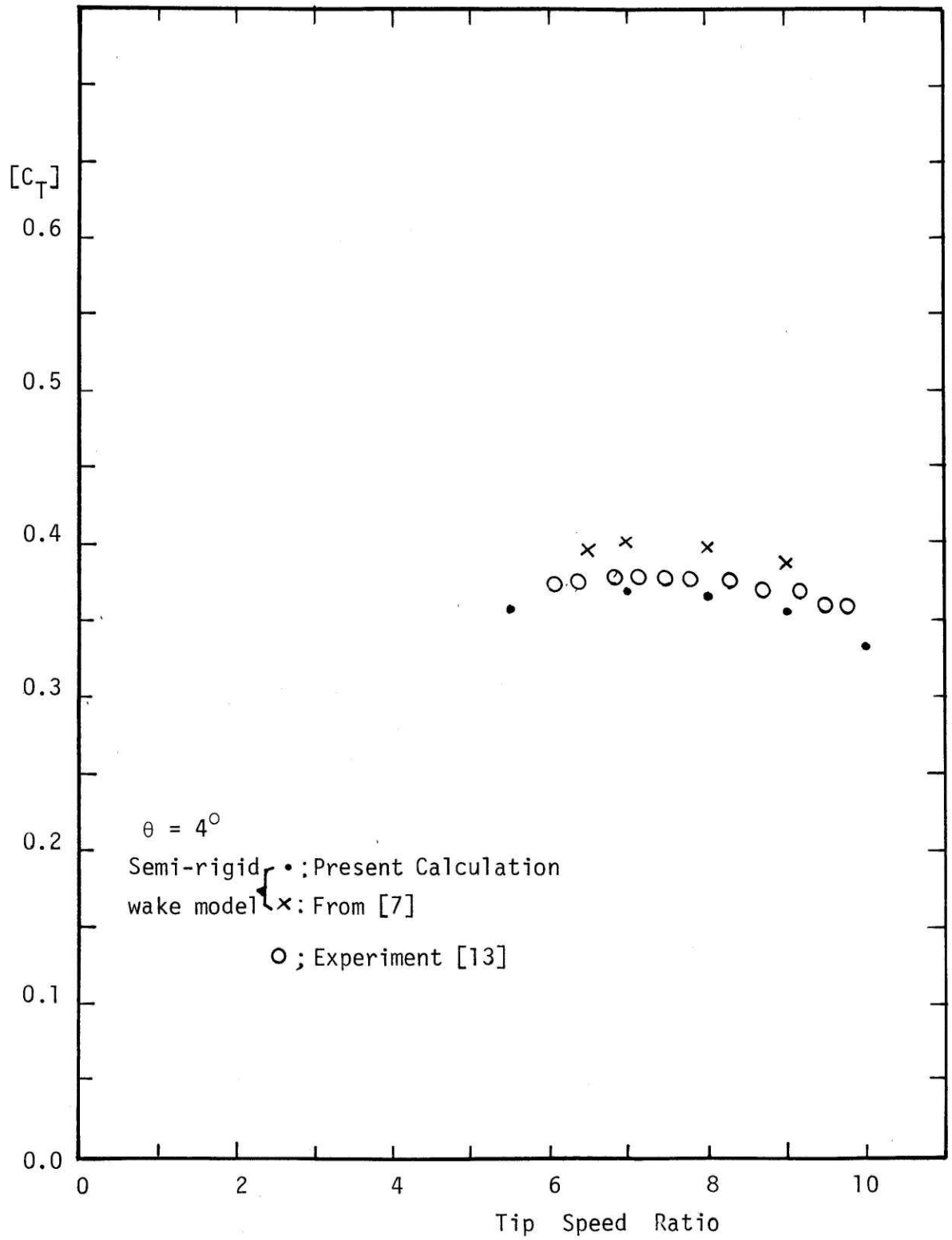

<Fig.5.6>Comparison of Present Lifting Line Theory and Previous One

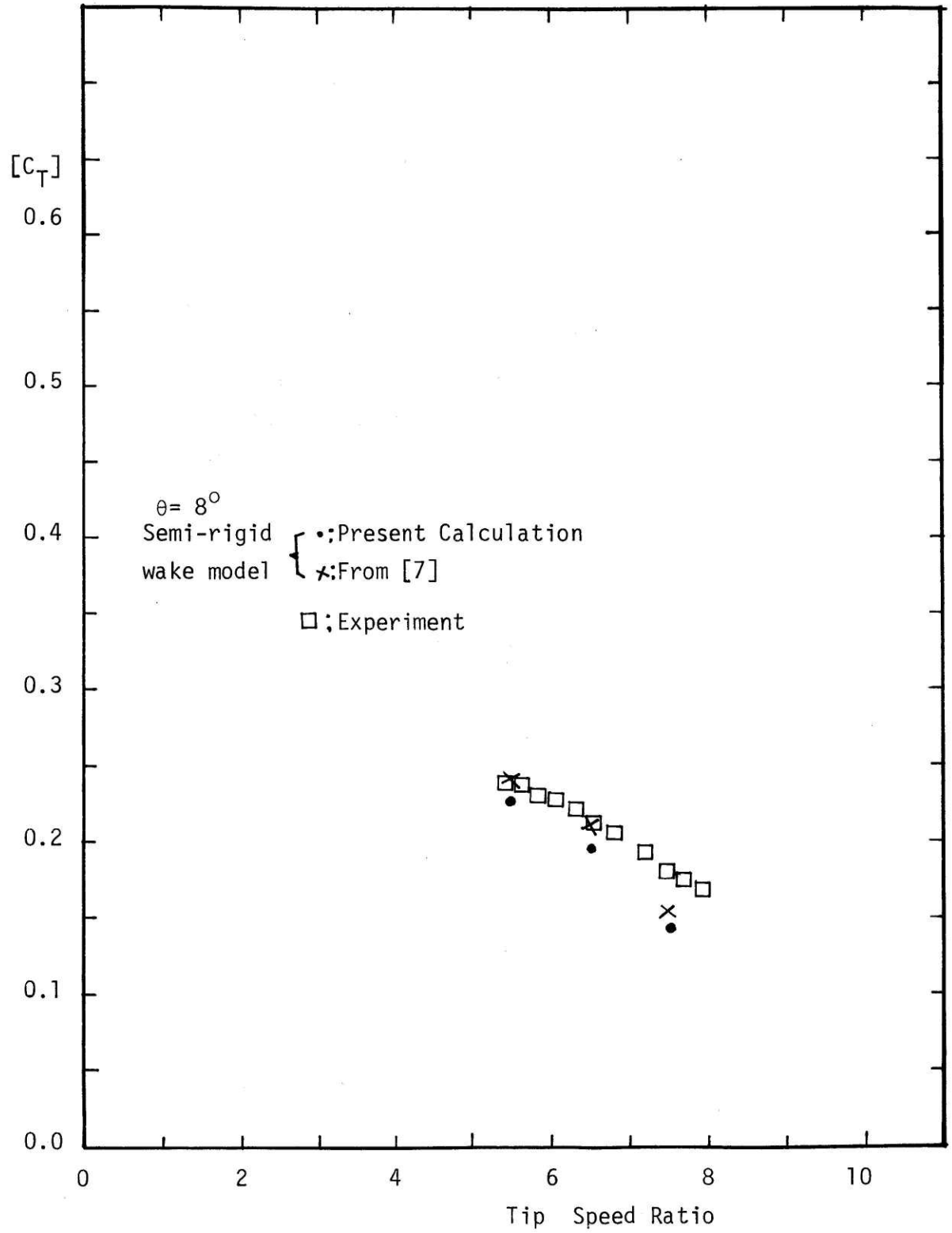

<Fig.5.7> Comparison of Present Lifting Line Theory and the Previous One

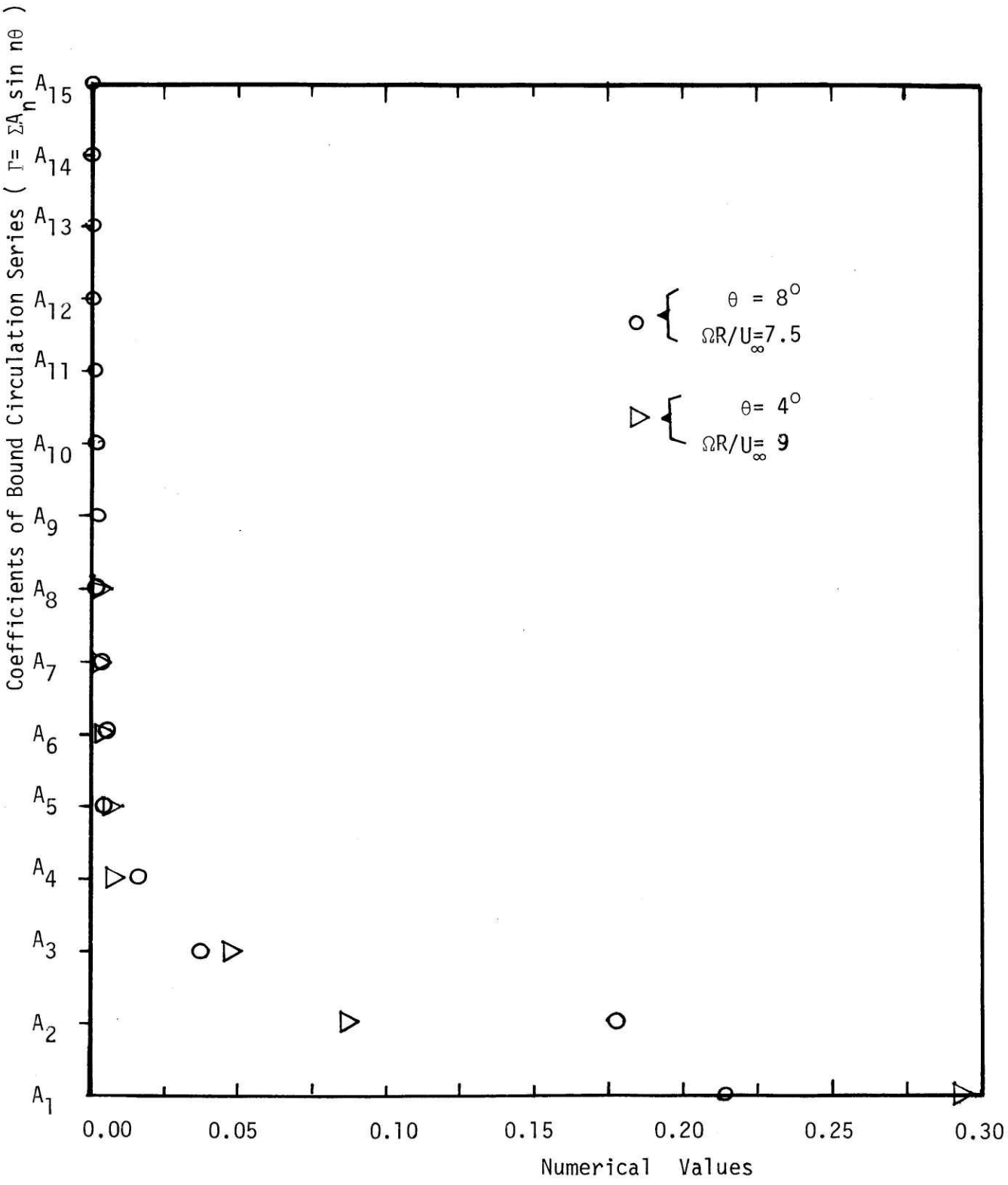

<Fig. 5.8>Numerical Values of the Coefficients of the Bound Circulation Series for Typical Cases

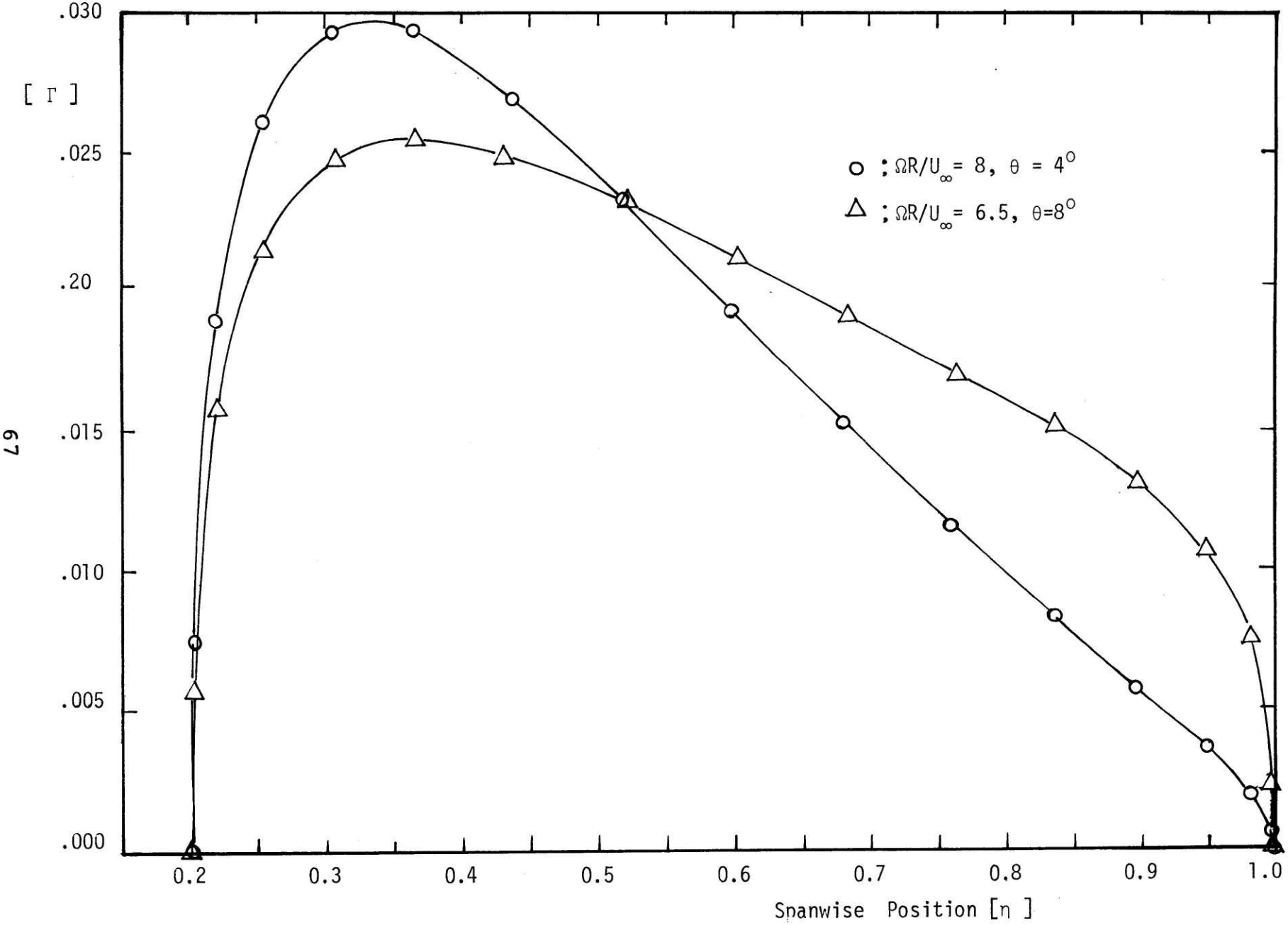

<Fig.5.9>Bound Circulation Distribution along the Blade

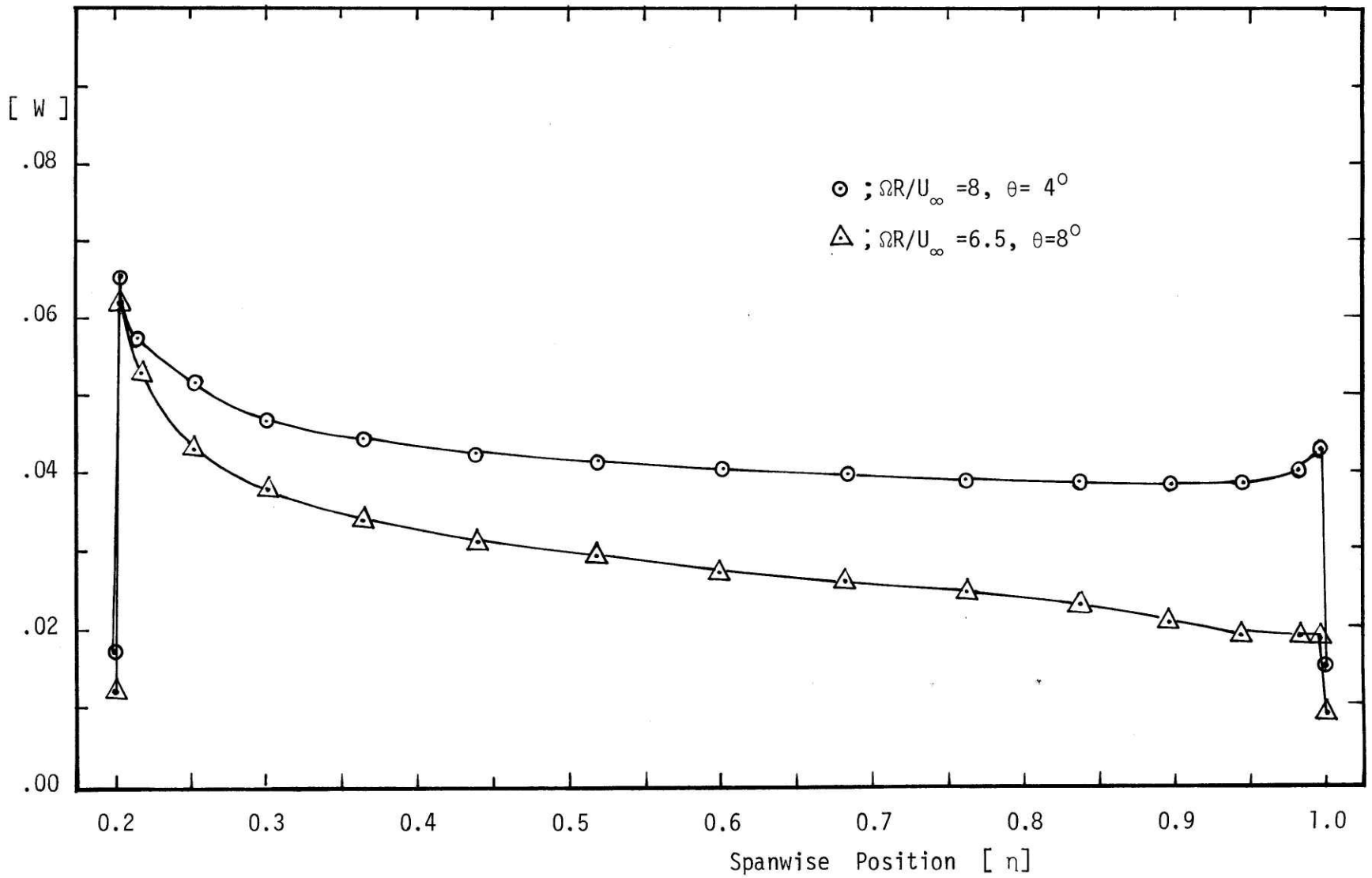

<Fig.5.10>Induced Velocity Distribution along the Blade

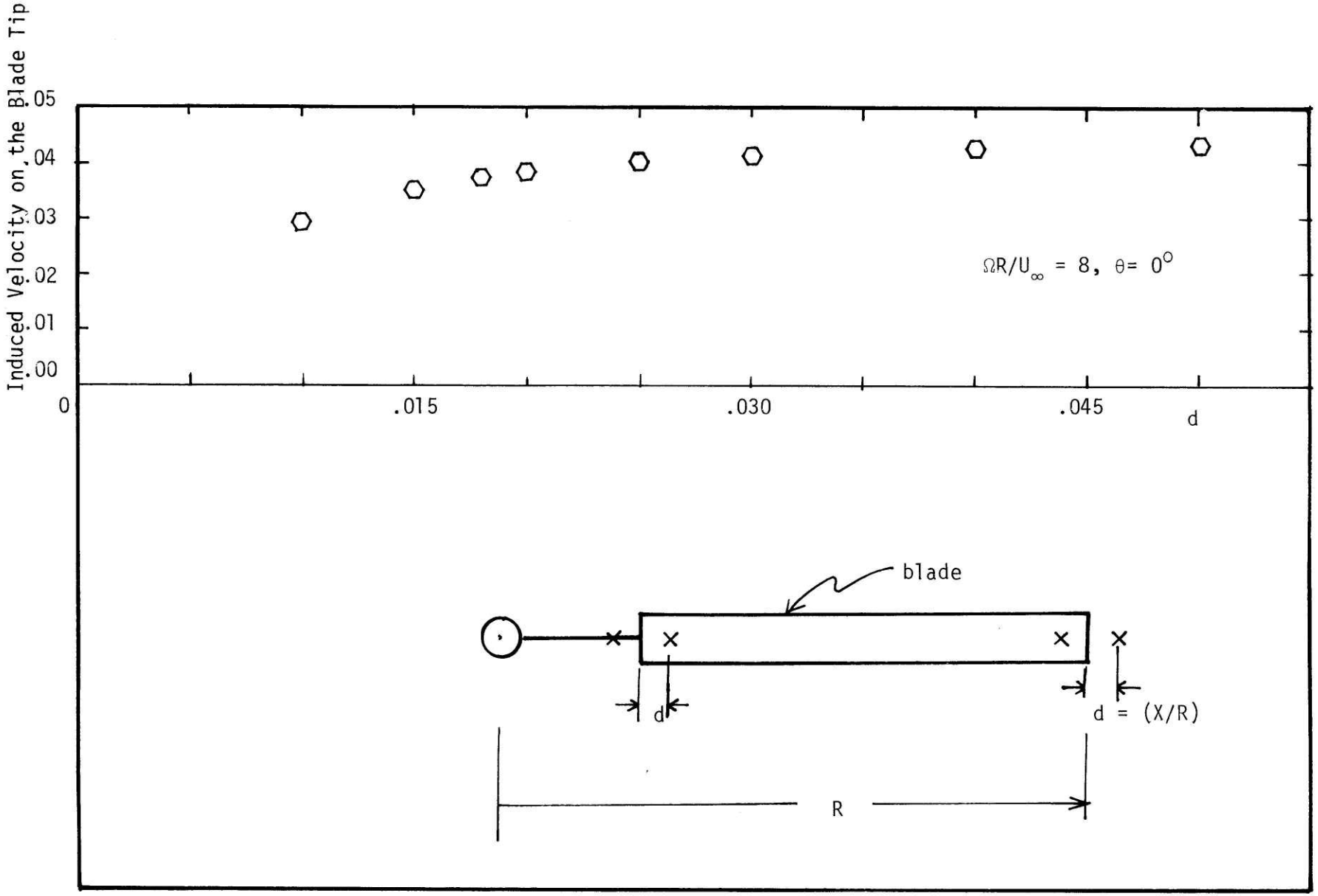

〈Fig.5.1〉 Induced Velocity on the Blade Tip as a Function of Radial Distance d.

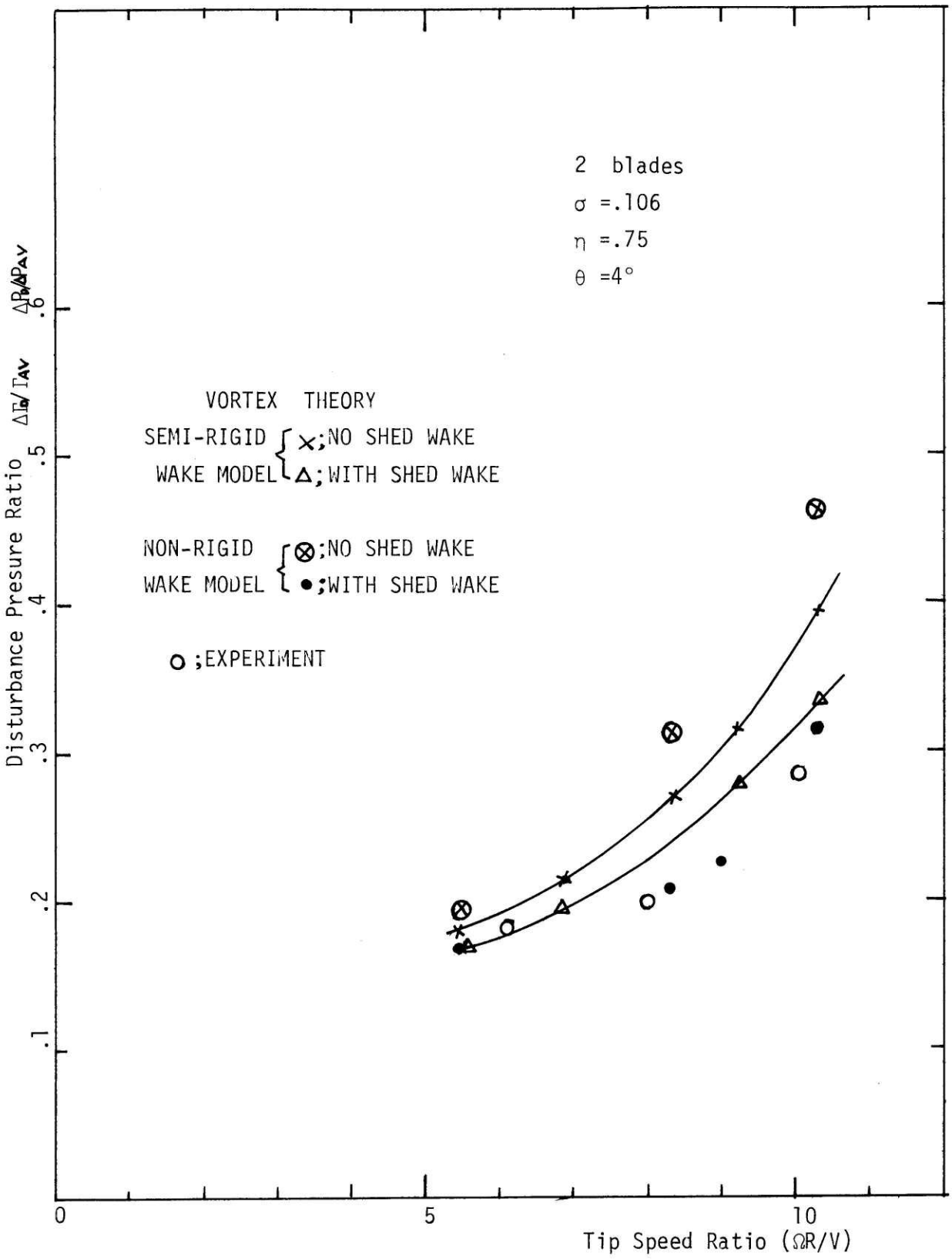

<Fig.5.12>Comparison of Theory and Experiment
(Disturbance Presure Ratio)

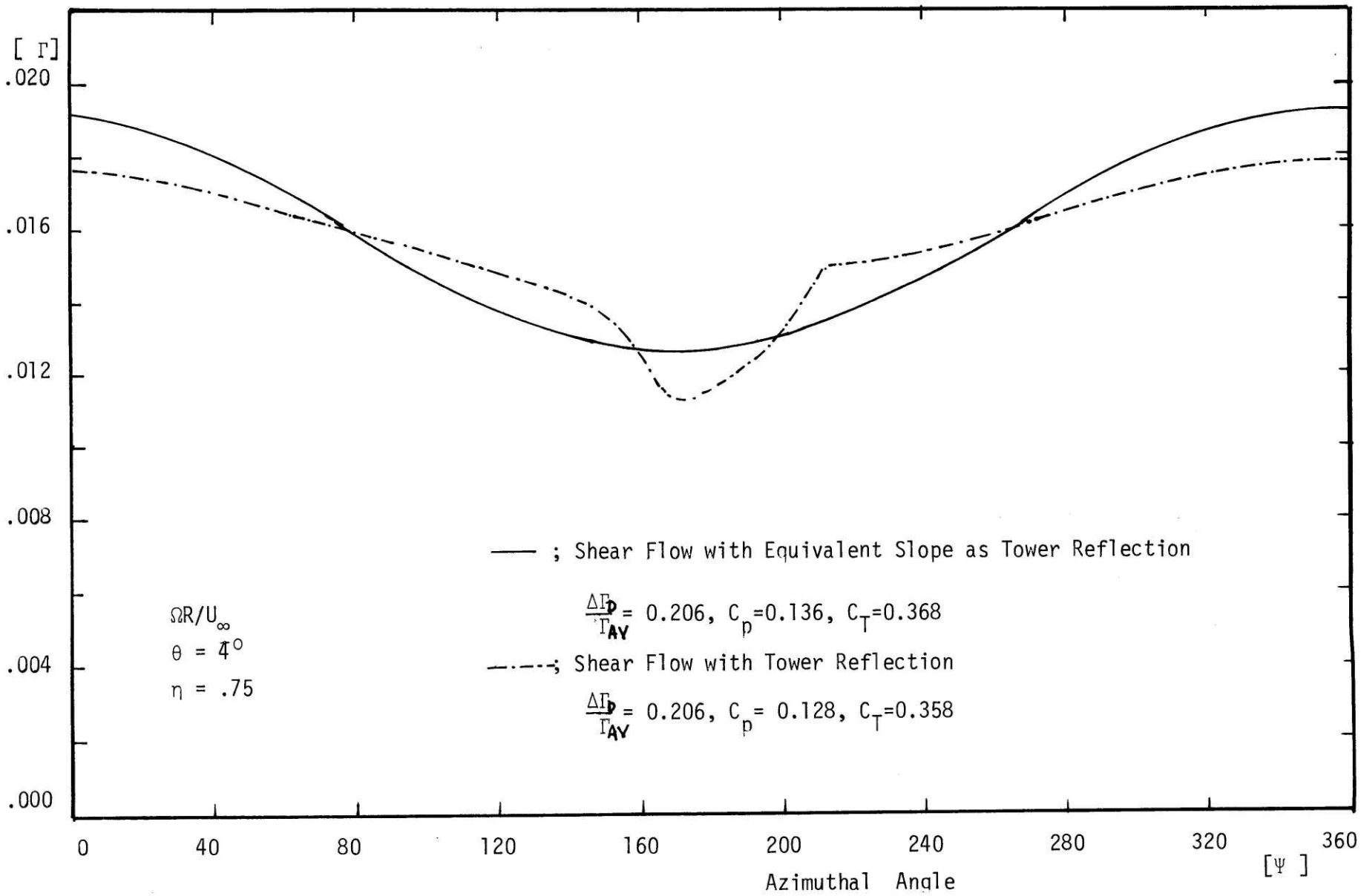

<Fig.5.13>Comparison of Bound Circulation of Net Shear Flow and of Shear Flow with Tower Reflection

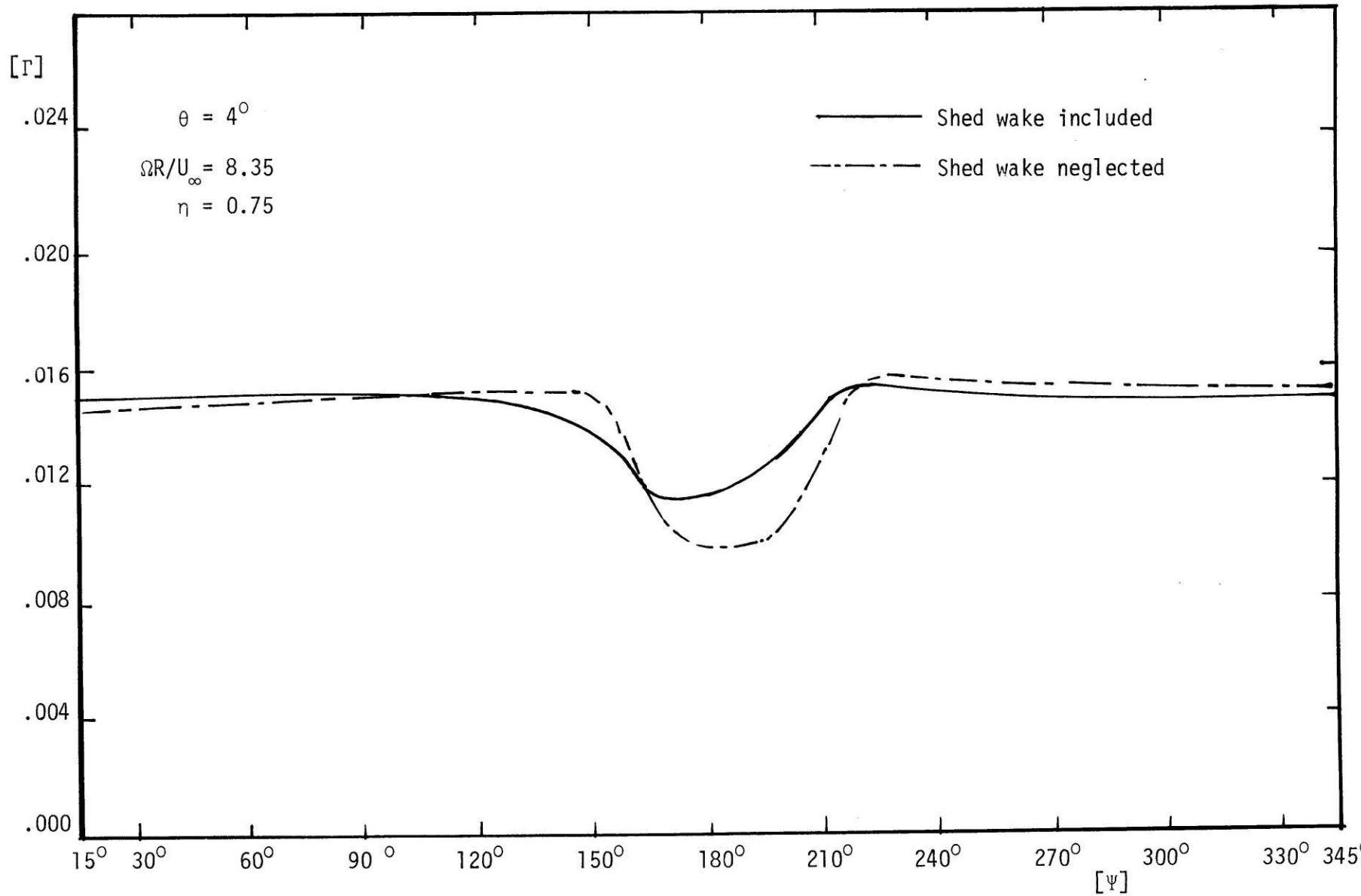

<Fig.5.14>Bound Circulation along Azimuthal Angle for the Tower Reflection with Uniform Free Stream

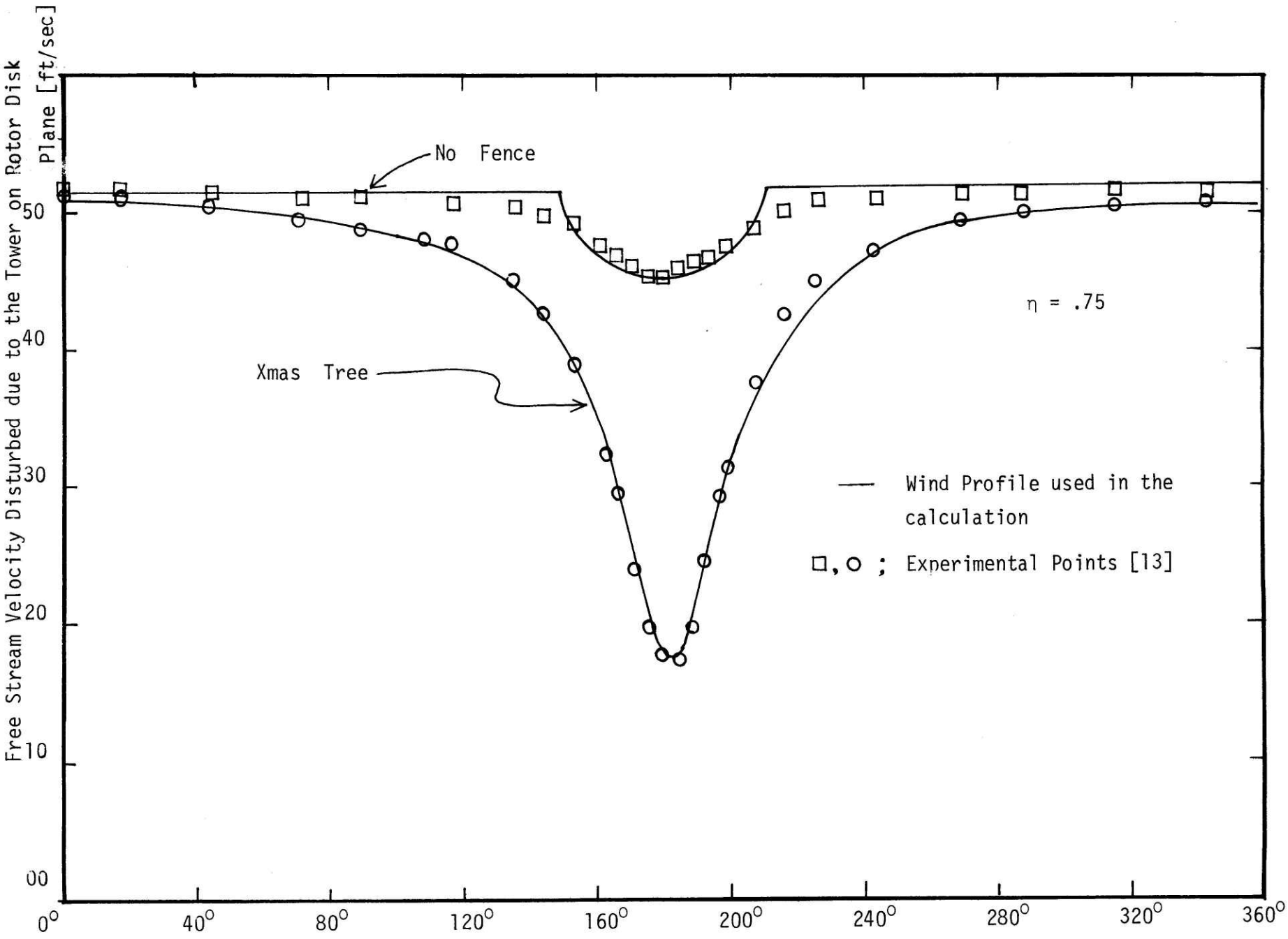

<Fig.5.15>Wind Profile Used in the Analysis and Experimental Points

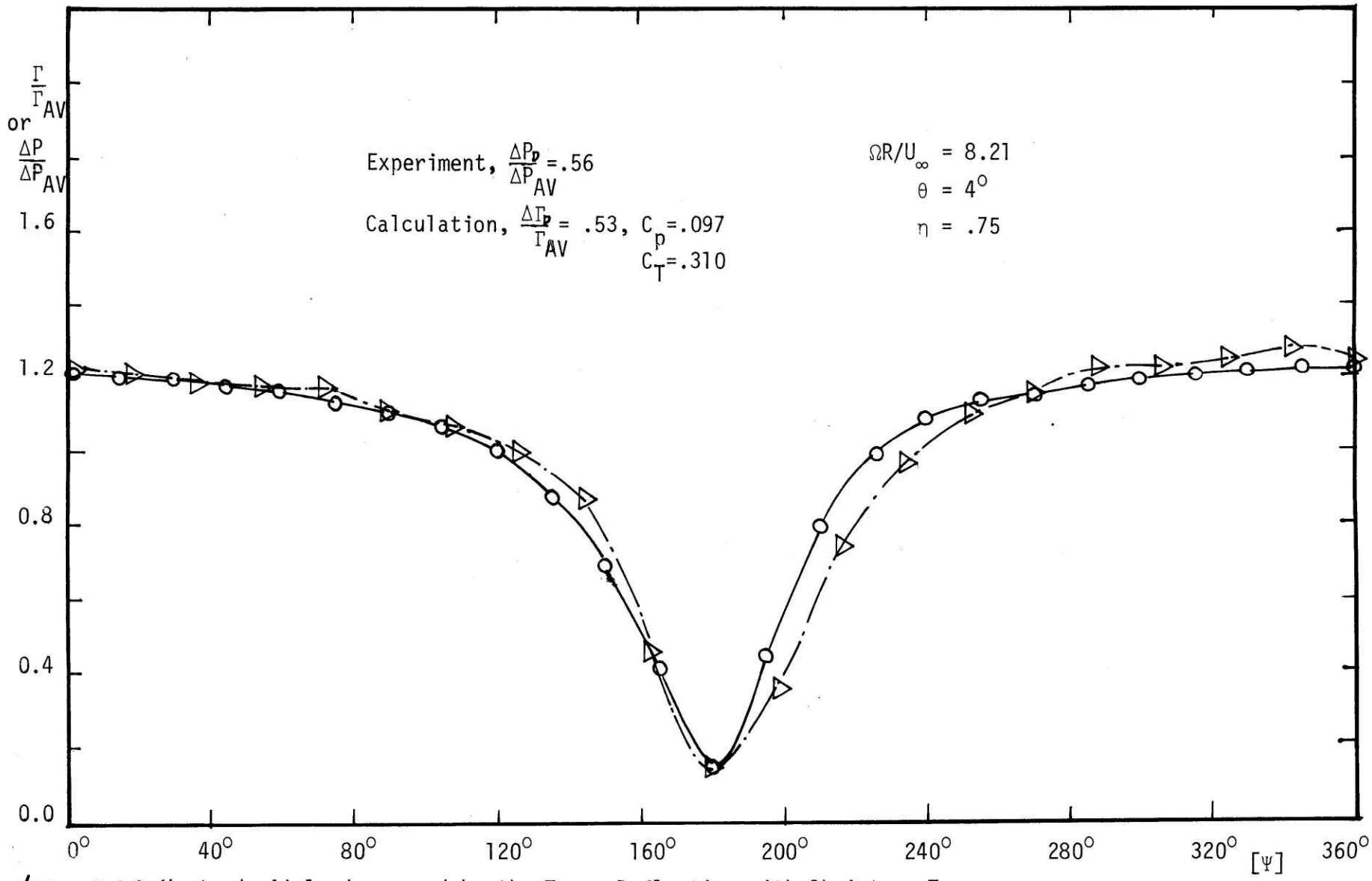

⟨Fig. 5.16⟩ Unsteady Airloads caused by the Tower Reflection with Christmas Tree

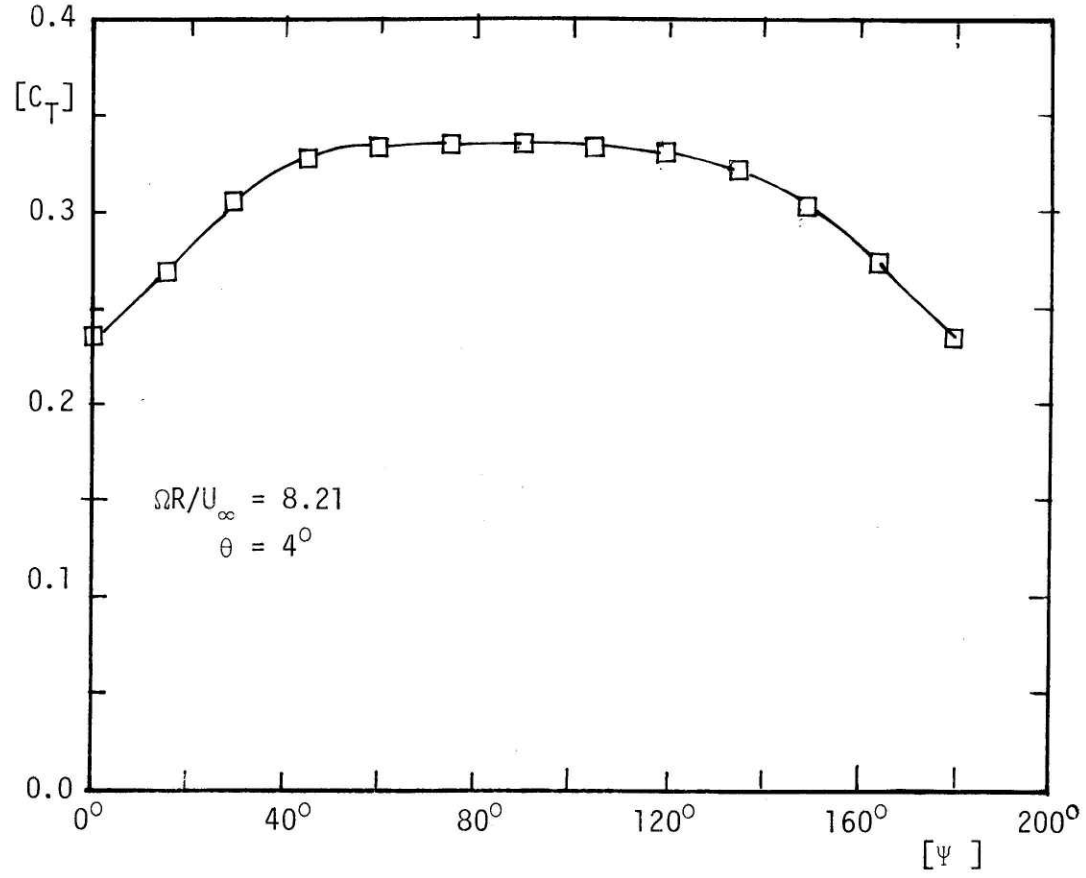

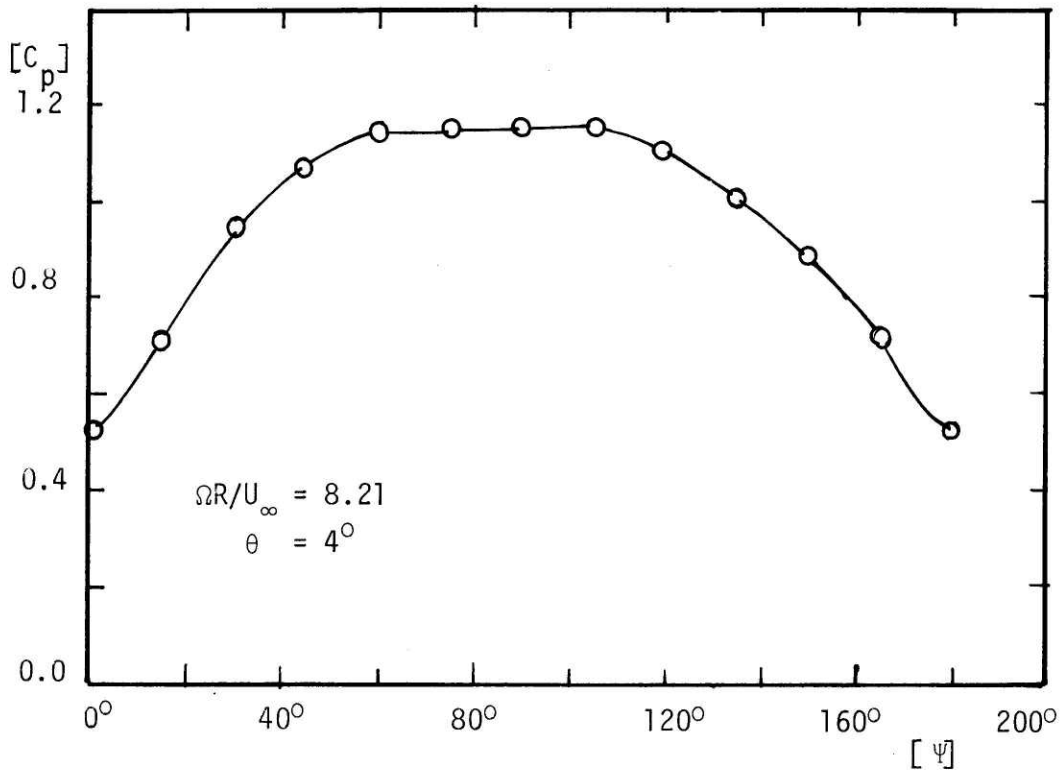

<Fig.5.17> Instantaneous Power **and** Thrust Coefficients of the Rotor Operating in the Tower Reflection with Christmas Tree

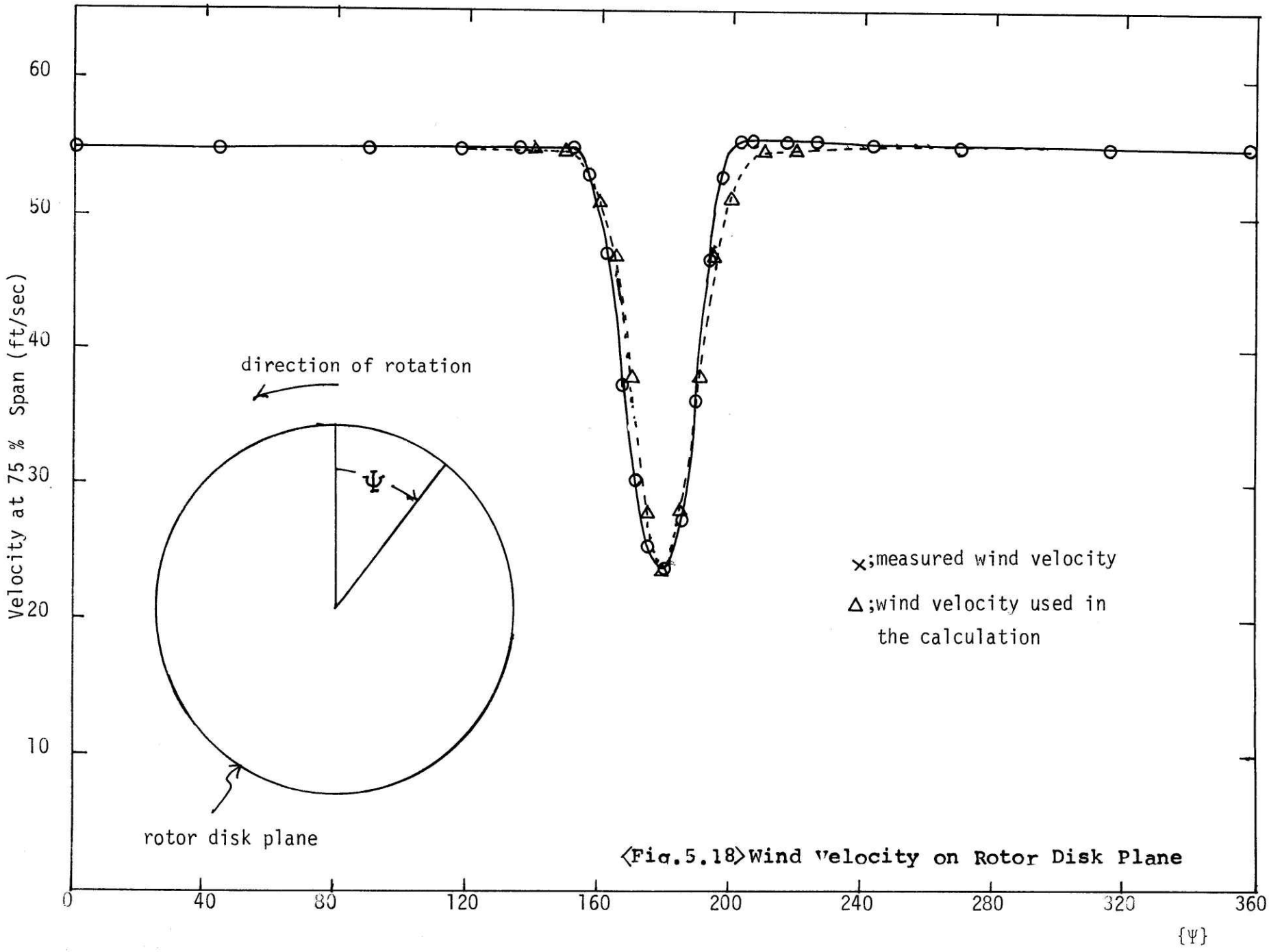

〈Fig.5.18〉Wind Velocity on Rotor Disk Plane

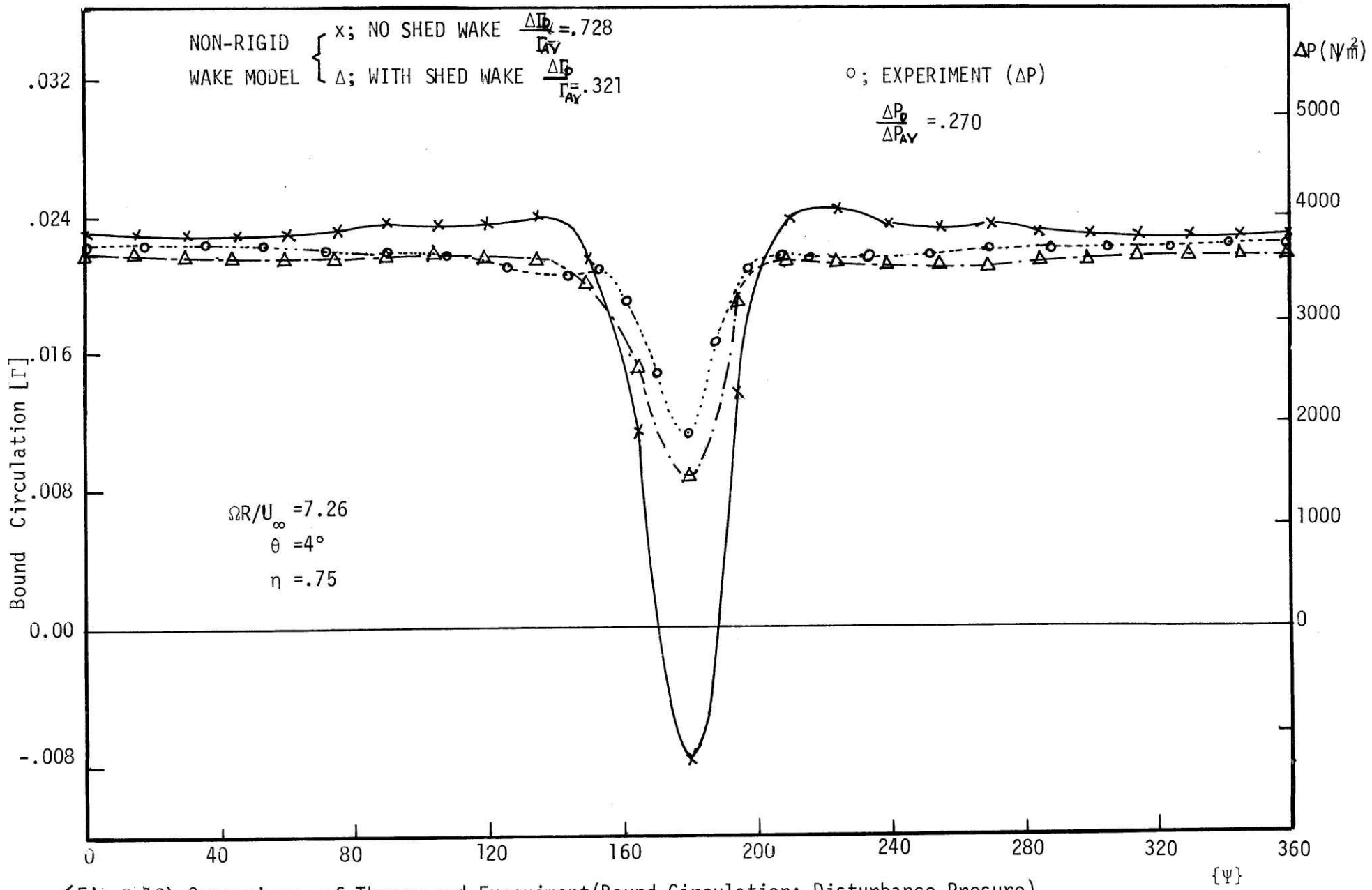

77

〈Fig.5.19〉 Comparison of Theory and Experiment(Bound Circulation: Disturbance Presure)

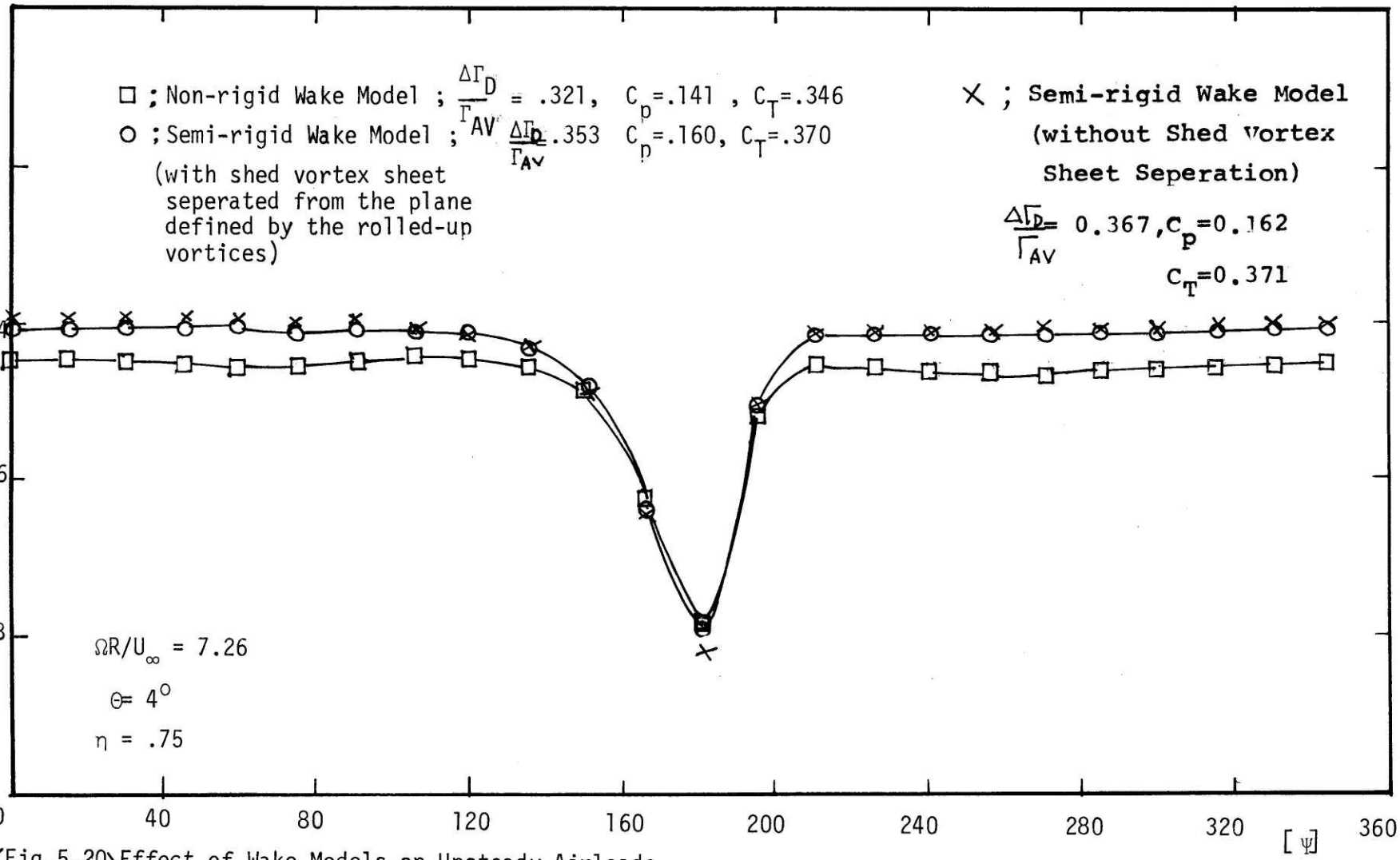

<Fig.5.20>Effect of Wake Models on Unsteady Airloads

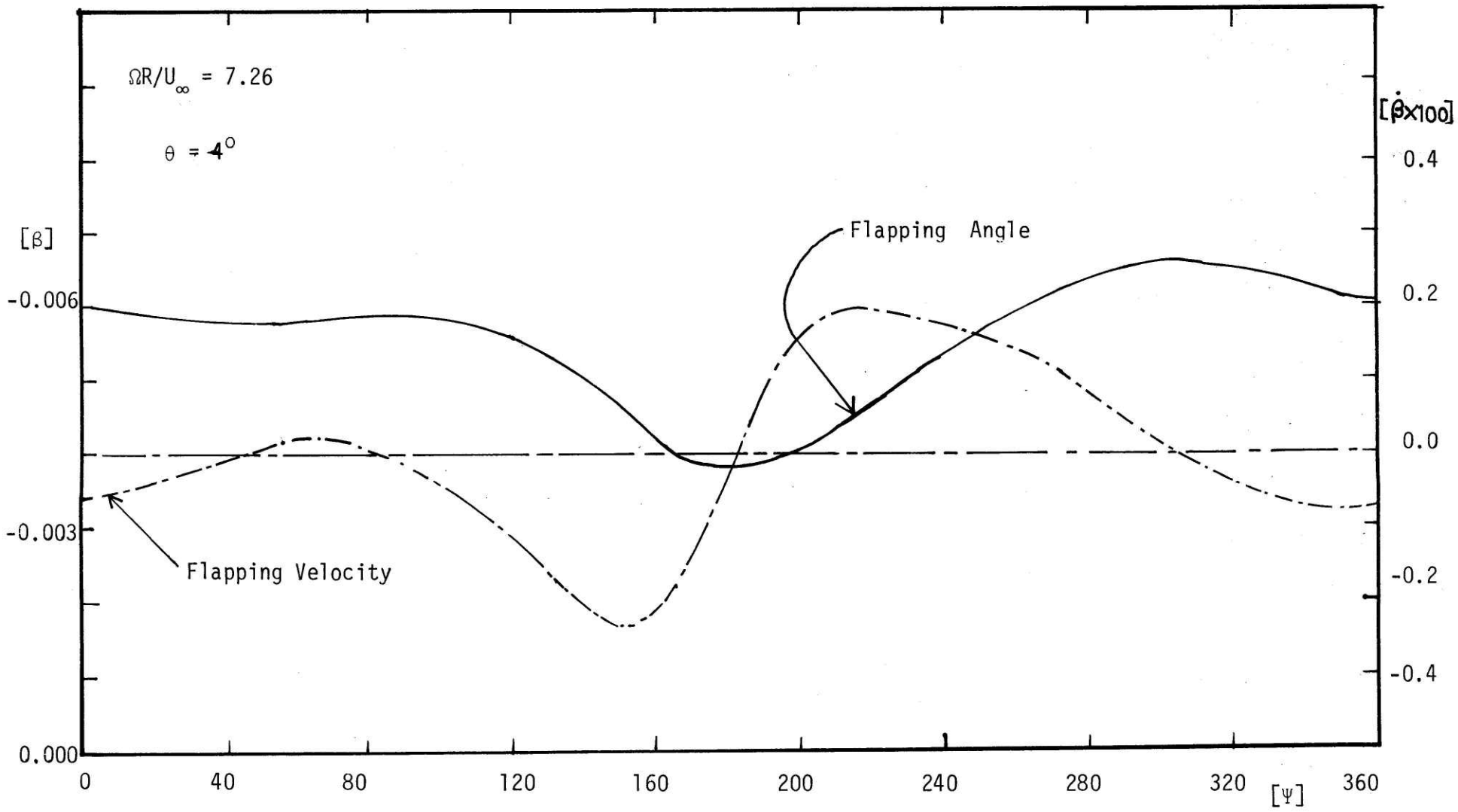

<Fig.5.21> Rigid Body Flapping Angle and Flapping Velocity for the Tower Shadow Case.

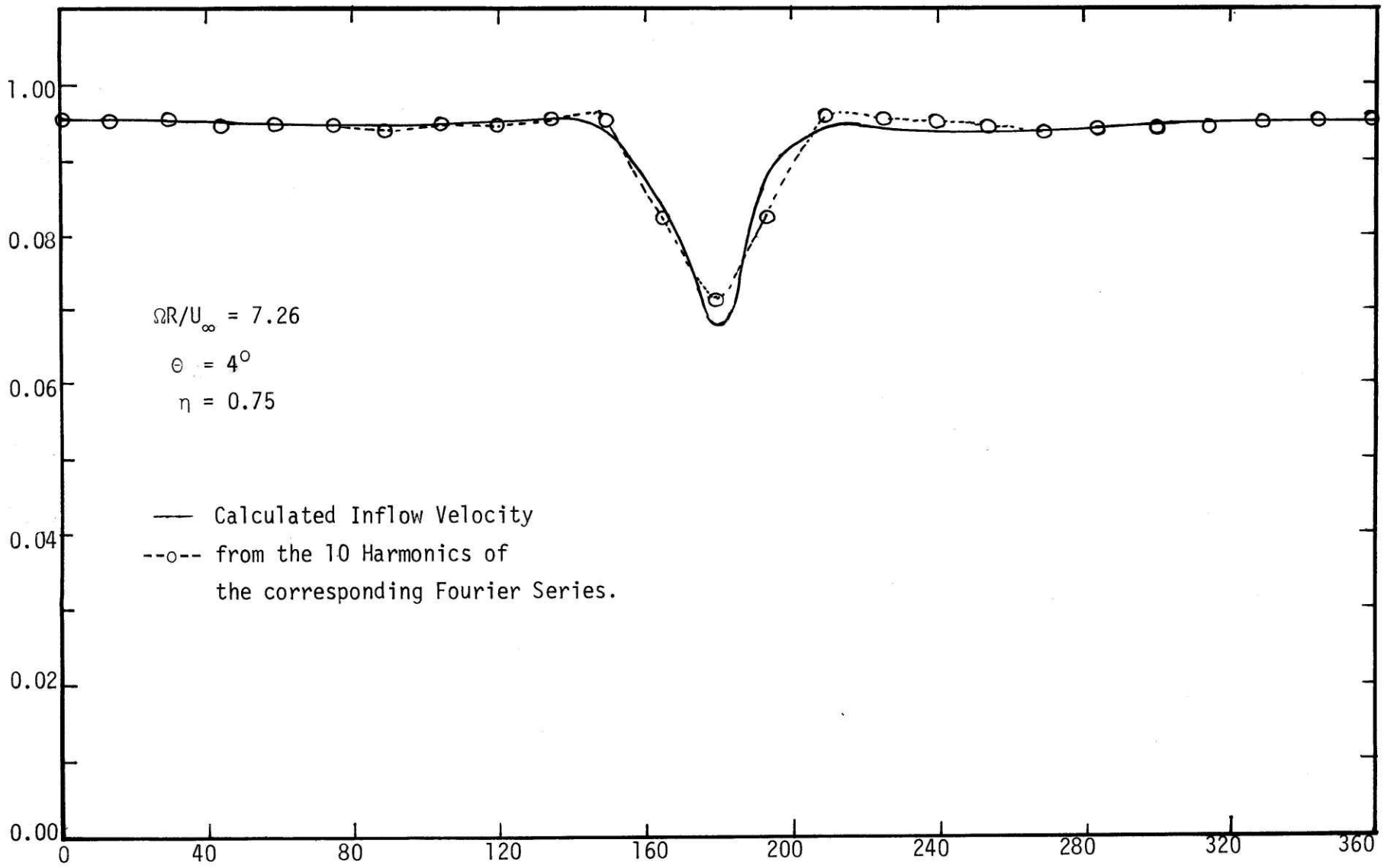

<Fig. 5.22>The Inflow Velocity and the One Computed from the 10 Harmonics of the Corresponding Series.

Appendix A

CALCULATION OF INFLUENCE COEFFICIENTS C_{ij}

A influence coefficient C_{ij} gives the velocity induced at i-th control point by the wake which is generated from j-th component of bound circulation series, and of unit amplitude. The induced velocity (W_i) at i-th control point is $\sum_j A_j \cdot C_{ij}$. From the application of the Biot-Savart Law to the wake whose geometry is determined from the previous induced velocity distribution on blade, one can compute influence coefficients C_{ij} as follows.

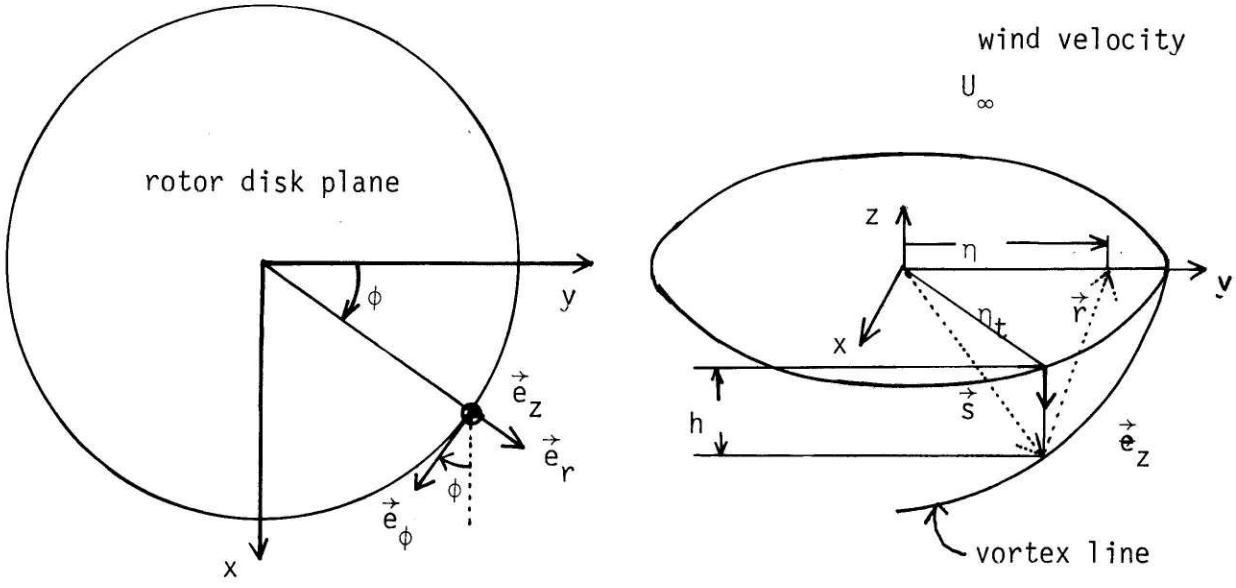

<Fig. A.1> Geometry for the Calculation of C_{ij}

h ; axial distance from the rotor disk plane to a vortex line.

$\vec{r} = \eta \vec{j} - \vec{s}$, $\vec{s} = \eta_t \vec{e}_r + h \vec{e}_z$ ($\vec{e}_z = -\vec{k}$)

$$d\vec{W}(\eta) = -\frac{d\Gamma}{4\pi} \int_0^{n \text{ spirals}} \frac{\vec{r} \times d\vec{S}}{|\vec{r}|^3} \qquad \text{(A.1)}$$

This equation gives the induced velocity due to a line vortex of strength $d\Gamma$ and of n spirals.

$$\frac{d\vec{S}}{d\phi} = \frac{d\eta_t}{d\phi}\vec{e}_r + \eta_t \frac{d\vec{e}_r}{d\phi} + \frac{dh}{d\phi}\vec{e}_z$$

$\vec{r}$; a position vector from a point on the vortex line to the position of the blade at which the induced velocity is computed

$$d\vec{S} = (w_r \vec{e}_r + \eta_t \vec{e}_\phi + V \vec{e}_z)\, d\phi$$

w_r ; outward radial induced velocity on a vortex line

V ; axial velocity of a trailing vortex

$$\vec{r} \times d\vec{S} = \{\eta_t^2 - \eta(w_r \sin\phi + \eta_t \cos\phi)\}\vec{k} + \{(\eta_t V - h w_r)\cos\phi + h\eta_t \sin\phi - \eta V\}\vec{i} + \{-(\eta_t V - h w_r)\sin\phi + h\eta_t \cos\phi\}\vec{j} \qquad (A.2)$$

$$|\vec{r}|^2 = \eta^2 + \eta_t^2 + h^2 - 2\eta\eta_t \cos\phi \qquad (A.3)$$

From equations(A.1),(A.2),and(A.3),three components of the induced velocity are derived.

$$d w_z = \frac{d\Gamma}{4\pi}\int_0^{2\pi n} \frac{\eta(w_r \sin\phi + \eta_t \cos\phi) - \eta_t^2}{(\eta^2 + \eta_t^2 + h^2 - 2\eta\eta_t \cos\phi)^{3/2}}\, d\phi \qquad (A.4)$$

$$d w_y = \frac{d\Gamma}{4\pi}\int_0^{2\pi n} \frac{(\eta_t V - h w_r)\sin\phi - \eta_t h \cos\phi}{(\eta^2 + \eta_t^2 + h^2 - 2\eta\eta_t \cos\phi)^{3/2}}\, d\phi \qquad (A.5)$$

$d w_x =$

Here, $V = U_\infty + W$ where U_∞ is the free stream velocity and W is the induced velocity on the tip vortex itself. Assuming that W is linearly varying up to k_1 spiral of vortex line and after k_1 spiral is constant as discussed in section 2.2, W is obtained as follows.

$$w = w_0 + \frac{\phi}{2\pi k_1} \cdot w_0 \cdot RD = w_0 + \frac{w_0 \cdot RD}{2\pi k_1} \cdot \phi_0 + \frac{w_0 RD}{2\pi k_1} \cdot x^* = \alpha_2 + \beta_2 x^* \tag{A.6}$$

, where W_0 is the induced velocity of a trailing vortex when it is trailed, RD is a parameter of the change of W after k_1 spiral. Then, when $\phi \leqq 2\pi k_1$

$$V = (U_\infty + w_0) + \frac{\phi}{2\pi k_1} w_0 \cdot RD$$

$$\therefore h = (U_\infty + w_0)\phi + \frac{\phi^2}{4\pi k_1} \cdot w_0 \cdot RD \tag{A.7}$$

By permitting small variations in ϕ around ϕ_0, h is given by

$$h = (U_\infty + w_0)(\phi_0 + x^*) + \frac{w_0 RD}{4\pi k_1} (\phi_0 + x^*)^2$$

$$\therefore h = \alpha_1 + \beta_1 \cdot x^* + \gamma_1 x^{*2} \tag{A.8}$$

$$h^2 = \alpha_1^2 + 2\alpha_1\beta_1 + (\beta_1^2 + 2\alpha_1\gamma_1) x^{*2} + (\quad) x^{*3} + (\quad) x^{*4} \tag{A.9}$$

When $\phi > 2\pi k_1$, $w = (1 + RD) w_0$

$$h = h_0 + (U_\infty + w)\phi' \quad , \quad \phi' = \phi - 2\pi k_1$$

$$\therefore h = h_0 - \{U + w_0(1+RD)\} 2\pi k_1 + \{U + w_0(1+RD)\}\phi$$

From equation (7) $h_0 = \pi k_1 \{2U + w_0(2+RD)\}$

$$h = -RD\, w_0 \pi k_1 + \{U + w_0(1+RD)\}(\phi_0 + x^*)$$

$$= \alpha_2 + \beta_2 x^* \tag{A.10}$$

$$h^2 = \alpha_2^2 + 2\alpha_2\beta_2 x^* + \beta_2^2 x^{*2} \tag{A.11}$$

Likewise W_r is assumed to vary linearly.

$$w_r = w_{ro} - \frac{\phi}{2\pi k_2} w_{ro}$$

, where W_{ro} is the radial induced velocity of the tip vortex on the rotor disk plane. After k_2 spirals of the tip vortex, W_r is zero.

$$w_r = w_{ro} - \frac{w_{ro}\phi_o}{2\pi k_2} - \frac{w_{ro}}{2\pi k_2} \chi^*$$

$$= \alpha_1 + \beta_1 \chi^* \qquad \text{(A.12)}$$

The radial position of the tip vortex is defined by η_t.

$$\eta_t = \eta_{to} - w_{ro}\phi - \frac{\phi^2}{4\pi k_2} w_{ro}$$

where η_{to} is the radial position when the tip vortex is trailed. Substitution of ϕ with $(\phi_o + \chi^*)$ into the above equation gives

$$\eta_t = \eta_{to} + w_{ro}\phi_o - \frac{w_{ro}}{4\pi k^2}\phi^2 + \left(w_{ro} - \frac{w_{ro}\phi_o}{2\pi k_2}\right)\chi^* - \frac{w_{ro}}{4\pi k_2}\chi^{*2}$$

$$= \alpha_3 + \beta_3 \chi^* + \gamma_3 \chi^{*2} \qquad \text{(A.13)}$$

$$\eta_t^2 = \alpha_3^2 + 2\alpha_3\beta_3 \chi^* + (\beta_3 + 2\alpha_3\gamma_3)\chi^{*2} \qquad \text{(A.14)}$$

$$\cos\phi = \cos(\phi_o + \chi^*) = \cos\phi_o - \sin\phi_o \cdot \chi^* - \frac{1}{2}\cos\phi_o \cdot \chi^{*2}$$

$$= p - q \cdot \chi^* - \frac{1}{2} p \cdot \chi^{*2} \qquad \text{(A.15)}$$

$$\sin\phi = \sin(\phi_o + \chi^*)$$

$$= q + p\chi^* - \frac{1}{2} q \cdot \chi^{*2} \qquad \text{(A.16)}$$

From equations (A.13), (A.14) and (A.15), $(\eta^2+\eta_t^2-2\eta\eta_t\cos\phi)$ term is obtained to the second order of x^*.

$$\begin{aligned}\eta^2+\eta_t^2-2\eta\eta_t\cos\phi &\doteq \eta^2+\alpha_3^2-2\eta\alpha_3 p+2\{\alpha_3\beta_3+\eta(\alpha_3 q-\beta_3 p)\}x^* \\ &\quad +2\{\alpha_3\gamma_3+\beta_3^2/2+\eta(\tfrac{1}{2}\alpha_3 p-\gamma_3 p+\beta_3 q)\}x^{*2} \\ &= a+2b\,x^*+c\,x^{*2} \qquad (A.17)\end{aligned}$$

(i). $\phi \leqq 2\pi - k_1$

From equations (A.9) and (A.17),

$$\begin{aligned}*\ \eta^2+\eta_t^2+h^2-2\eta\eta_t\cos\phi &= (\alpha_1^2+a)+2(\alpha_1\beta_1+b)x^*+(\beta_1^2+2\alpha_1\gamma_1+c)x^{*2} \\ &= A+2B\,x^*+C\,x^{*2} \qquad (A.18)\end{aligned}$$

(ii). $\phi > 2\pi - k_1$

From equations (A.11) and (A.17),

$$\begin{aligned}*\ \eta^2+\eta_t^2+h^2-2\eta\eta_t\cos\phi &= \alpha_2^2+a+2(\alpha_2\beta_2+b)x^*+(\beta_2^2+c)x^{*2} \\ &= A+2B\,x^*+C\,x^{*2} \qquad (A.19)\end{aligned}$$

In the equation (A.4), $\eta(\eta_t\cos\phi+v\sin\phi)-\eta_t^2$ term is computed from equations (A.12), (A.13), (A.14), (A.15) and (A.16) to the second order of x^*.

$$\begin{aligned}*\ \eta(\eta_t\cos\phi+w_r\sin\phi)-\eta_t^2 &= \eta(\alpha_3 p+\ell_1 q)-\alpha_3^2+\{\eta(-\alpha_3 q+\beta_3 p+\ell_1 p+t_1 q) \\ &\quad -2\alpha_3\beta_3\}x^* = D+E\,x^* \qquad (A.20)\end{aligned}$$

In the equation (A.5) $* (\eta_t V - h w_r) \sin\phi - \eta_t h \cos\phi$ term is obtained as follows.

(i). $\phi \leqq 2\pi k_1$

From the equations (A.6), (A.8), (A.12), (A.13), (A.15), and (A.16),

$$
\begin{aligned}
&(\eta_t V - h w_r)\sin\phi - \eta_t h \cos\phi \\
&= q\{\alpha_3(U+\rho_2) - \alpha_1\rho_1\} - \alpha_3\alpha_1 p \\
&\quad + [\, p\{\alpha_3(U+\rho_2) - \alpha_1\rho_1\} - \alpha_1\rho_1\} \\
&\qquad + q\{\alpha_3 t_2 + \beta_3(U+\rho_2) - \alpha_1 t_1 - \beta_1\rho_1\} \\
&\qquad - \alpha_3\beta_1 p - \beta_3\alpha_1 p + \alpha_3\alpha_1 q\,]\, x^* \\
&= F + G x^* \qquad \text{(A.21)}
\end{aligned}
$$

(ii). $\phi > 2\pi k_1$

$$\rho_2 = w_0(1+RD),\ t_2 = 0 \quad \& \quad h = \alpha_2 + \beta_2 x^*$$

Equations (A.18), (A.19), (A.20), and (A.21) give the final form of equation to compute induced velocities.

$$dw_z = \frac{d\Gamma}{4\pi}\sum_{\phi}\int_{-\Delta\phi_0}^{\Delta\phi_0}\frac{D + E x^*}{[A + 2Bx^* + C x^{*2}]^{3/2}}\,dx^* = \frac{d\Gamma}{4\pi}\sum_{\phi} I_1$$

$$dw_y = \frac{d\Gamma}{4\pi}\sum_{\phi}\int_{-\Delta\phi_0}^{\Delta\phi_0}\frac{F + G x^*}{[A + 2Bx^* + C x^{*2}]^{3/2}}\,dx^* = \frac{d\Gamma}{4\pi}\sum I_2$$

$$\eta = \eta_{rc} + \frac{1}{2}(1 - \cos\theta)$$

$$\Gamma(\eta) = \sum_n A_n \sin n\theta$$

$$d\Gamma(\eta) = \sum(-n A_n)\cos n\theta\, d\theta$$

$$w_z = \frac{1}{4\pi} \sum_n (-n A_n) \sum_j \sum_i \cos n\theta \, I_1 \cdot 2\Delta\theta_0 = \sum_n A_n C_n = w \qquad \text{(A.22)}$$

$$w_y = \frac{1}{4\pi} \sum (-n A_n) \sum_j \sum_i \cos n\theta I_2 \cdot 2\Delta\theta_0 = \sum_n A_n D_n = w_{ro} \qquad \text{(A.23)}$$

$$\phi = (2i-1)\Delta\phi_0 , \quad \theta = (2j-1)\cdot\Delta\theta_0$$

$$I_1 = \int_{-\Delta\phi_0}^{\Delta\phi_0} \frac{(D + E x^*)}{[A + 2B x^* + C x^{*2}]^{3/2}} \cdot dx^* ,$$

$$I_2 = \int_{-\Delta\phi_0}^{\Delta\phi_0} \frac{(D + E x^*)}{[A + 2B x^* + C x^{*2}]^{3/2}} \cdot dx^* \qquad \text{(A.24)}$$

Appendix B

ALL COEFFICIENTS USED IN CALCULATING C_{ij}

If $AC \neq B^2$

$$I_1 = \frac{1}{AC-B^2}\left[\frac{(DB - EA) + (DC - EB)\Delta\phi_0}{\sqrt{A + 2B\Delta\phi_0 + C\Delta\phi_0^2}} - \frac{(DB - EA) - (DC - EB)\Delta\phi_0}{\sqrt{A - 2B\Delta\phi_0 + C\Delta\phi_0^2}}\right]$$

If $AC = B^2$

$$I_1 = \frac{EB - CD}{2\sqrt{C}}\left[\frac{1}{(B + C\cdot\Delta\phi_0)^2} - \frac{1}{(B - C\cdot\Delta\phi_0)^2}\right] + \frac{2E\cdot\Delta\phi_0\sqrt{C}}{B^2 - C^2\Delta\phi_0^2}$$

In I_2, D is replaced with F and E with G.

(i) $\phi \leqq 2\pi k_1$

$A = \alpha_1^2 + a, \quad B = \alpha_1\beta_1 + b, \quad C = \beta_1^2 + 2\alpha_1\gamma_1 + c$

(ii) $\phi > 2\pi k_1$

$A = \alpha_2^2 + a, \quad B = \alpha_2\beta_2 + b, \quad C = \beta_2^2 + c$

$D = \eta(\alpha_3 p + \rho_1 q) - \alpha_3^2$

$E = \eta(-\alpha_3 q + \beta_3 p + \rho_1 p + t_1 q) - 2\alpha_3\beta_3$

$F = q\{\alpha_3(U_\infty + \rho_2) - \alpha_1\rho_1\} - \alpha_3\alpha_1 p$

$G = p\{\alpha_3(U_\infty + \rho_2) - \alpha_1\rho_1\} + q\{\alpha_3 t_2 + \beta_3(U_\infty + \rho_2) - \alpha_1 t_1 - \beta_1\rho_1\}$
$- \alpha_3\beta_1 p - \beta_3\alpha_1 p + \alpha_3\alpha_1 q$

Here, when $\phi > 2\pi k_1$, then $\alpha_1 = \alpha_2$, $\beta_1 = \beta_2$.

$$\alpha_1 = (U_\infty + w_0)\phi + \frac{w_0 RD}{4\pi k_1}\phi^2$$

$$\alpha_2 = -RD\, w_0 \pi k_1 + \{U_\infty + w_0(1 + RD)\}\phi$$

$$\alpha_3 = \eta_{t0} + w_{r0}\phi - \frac{w_{r0}}{4\pi k_2}\phi^2$$

$$\beta_1 = U_\infty + w_0 + \frac{w_0 RD}{2\pi k_1}\phi^2$$

$$\beta_2 = U_\infty + w_0(1 + RD)$$

$$\beta_3 = w_{r0} - \frac{w_{r0}}{2\pi k_2}\phi$$

$$r_1 = \frac{w_0 RD}{4\pi k_1}$$

$$r_3 = -\frac{w_{r0}}{4\pi k_2}$$

$$p = \cos\phi$$

$$q = \sin\phi$$

$$\alpha_1 = w_{r0} - \frac{w_{r0}}{2\pi k_2}\phi \quad , \quad t_1 = -\frac{w_{r0}}{2\pi k_2}$$

$$\alpha_2 = w_0 + \frac{w_0 RD}{2\pi k_1}\phi \quad , \quad \text{if } \phi \geq 2\pi k_1 \quad \alpha_2 = (1+RD)w_0$$

$$t_2 = \frac{w_0 RD}{2\pi k_1} \quad , \text{ if } \phi \geq 2\pi k_1 \quad , \quad t_2 = 0$$

$$a = \eta^2 + \alpha_3^2 - 2\eta\alpha_3 p$$

$$b = \alpha_3\beta_3 + \eta(\alpha_3 q - \beta_3 p)$$

$$c = 2\{\alpha_3 r_3 + \beta_3^2/2 + \eta(\tfrac{1}{2}\alpha_3 p - r_3 p + \beta_3 q)\}$$

Appendix C

VELOCITY INDUCED BY A TRAILING OR SHED VORTEX ELEMENT

C.1 Trailing Vortex Element

The velocity W at position on the blade by a trailing vortex element A of strength $\Gamma(\phi)$ is obtained by applying the Biot-Savart formula. In vectorial form, the formula can be written as

$$\vec{W} = \frac{1}{4\pi} \int_{S_1}^{S_2} \Gamma(\phi) \frac{\vec{r} \times d\vec{s}}{r^3}$$

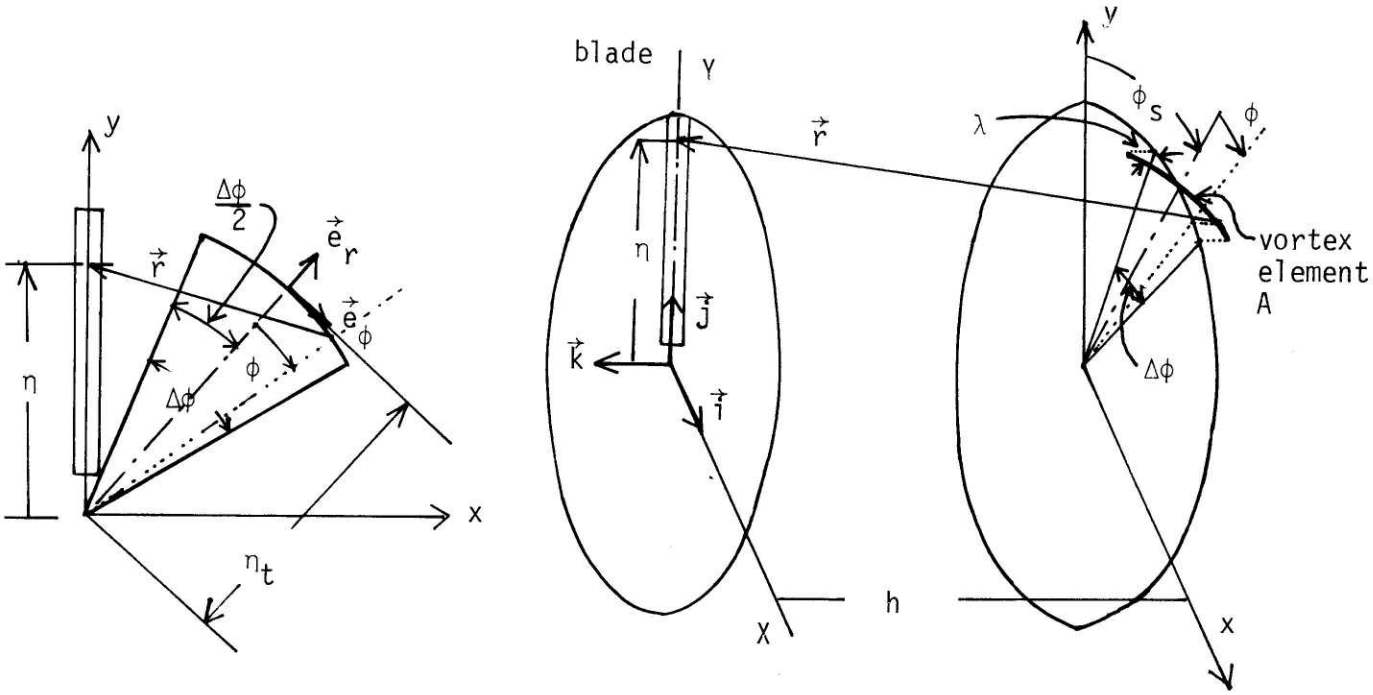

Projection to x-y Plane

<Fig. A.2> Geometry for the Calculation of the Velocity Induced by a Trailing Vortex

$\vec{e}_r, \vec{e}_\phi$ = unit vectors fixed at the midpoint of the vortex element.

λ = angle of inclination of the vortex element w.r. to X-Y plane.

h = axial distance from the X-Y plane to the midpoint of vortex element.

ϕ_s = azimuthal angle between the blade axis (j-axis) and the axis formed by the line from the orgin of x-y plane to midpoint.

Vortex element A in fig.A.2 is assumbed to be inclined w.r.to $\vec{e}_\phi$ by angle 'λ'.

$$\vec{r} = \eta \vec{j} - (\eta_t \vec{e}_r + \eta_t \phi \vec{e}_\phi - \eta_t \phi \tan(\lambda) \vec{k} - h \vec{k})$$

$$d\vec{s} = \eta_t d\phi \vec{e}_\phi - \eta_t d\phi \tan(\lambda) \vec{k} - \eta_t \phi d\phi \vec{e}_r$$

$$\tan(\lambda) = \frac{dh}{\eta_t d\phi}$$

$$\vec{r} \times d\vec{s} = [-(\eta - \eta_t \cos\phi_s)\eta_t \tan\lambda + h\eta_t \sin\phi_s] d\phi \vec{i} + (\eta_t^2 - \eta\eta_t \cos\phi_s) d\phi \vec{k} + [\phi(\eta\eta_t \sin\phi_s + \eta_t \phi)\vec{k} + \phi\eta_t (h + \eta_t \phi \tan\lambda) \vec{e}_\phi] d\phi$$

Linear variation of the strength of element A is assumed as follows.

$$\Gamma = \Gamma_t + \frac{\Delta\Gamma_t}{\eta\Delta\phi}\left(\phi + \frac{\Delta\phi}{2}\right) = \alpha + \phi\beta$$

$$W = \frac{1}{4\pi} \int_{\phi_1 = -\frac{\Delta\phi}{2}}^{\phi_2 = \frac{\Delta\phi}{2}} \frac{(\alpha+\beta\phi)\{(D\vec{i} + E\vec{k}) + (G\vec{i} + H\vec{k})\phi\} d\phi}{(ax^2 + 2bx + c)^{3/2}}$$

While neglecting the terms of order (ϕ^2) in the numerator, this equation becomes

(i). When $b^2 \neq ac$,

$$W = -\frac{\alpha}{4\pi}\left\{ (D\vec{i} + E\vec{K}) \left[\frac{ax + b}{(ac - b^2)\sqrt{ax^2+2bx+c}} \right]_{\phi_1}^{\phi_2} \right.$$

$$\left. + (G\vec{i} + H\vec{K}) \left[\frac{bx + c}{(b^2 - ac)\sqrt{ax^2+2bx+c}} \right]_{\phi_1}^{\phi_2} \right\}$$

(ii). When $b^2 = ac$,

$$W = -\frac{\alpha}{4\pi}\left\{ (D\vec{i} + E\vec{K}) \left[\frac{-\sqrt{a}}{2(ax+b)^2} \right]_{\phi_1}^{\phi_2} \right.$$

$$\left. + (G\vec{i} + H\vec{K}) \left[\frac{-1}{\sqrt{a}(ax+b)} + \frac{b}{2\sqrt{a}(ax+b)^2} \right]_{\phi_1}^{\phi_2} \right\}$$

In these expressions,

$$D = -(\eta - \eta_t \cos\phi_s)\eta_t \tan\lambda + h\eta_t \sin\phi_s$$

$$E = \eta_t^2 - \eta\eta_t \cos\phi_s$$

$$G = \eta_t h \cos\phi_s + \frac{\beta}{\alpha} D$$

$$H = \eta\eta_t \sin\phi_s + \frac{\beta}{\alpha} E$$

$$a = \eta_t^2 (1 + \tan^2\lambda)$$

$$b = \eta\eta_t \sin\phi_s + \eta_t h \tan\lambda$$

$$c = \eta_t^2 + \eta^2 + h^2 - 2\eta\eta_t \cos\phi_s$$

C.2 Shed Vortex Sheet and Element

The same equation as in [7] was used to calculate the velocity induced by a shed line vortex. For the shed vortex sheet, a slightly modified form of the equation for the shed line vortex element was used.

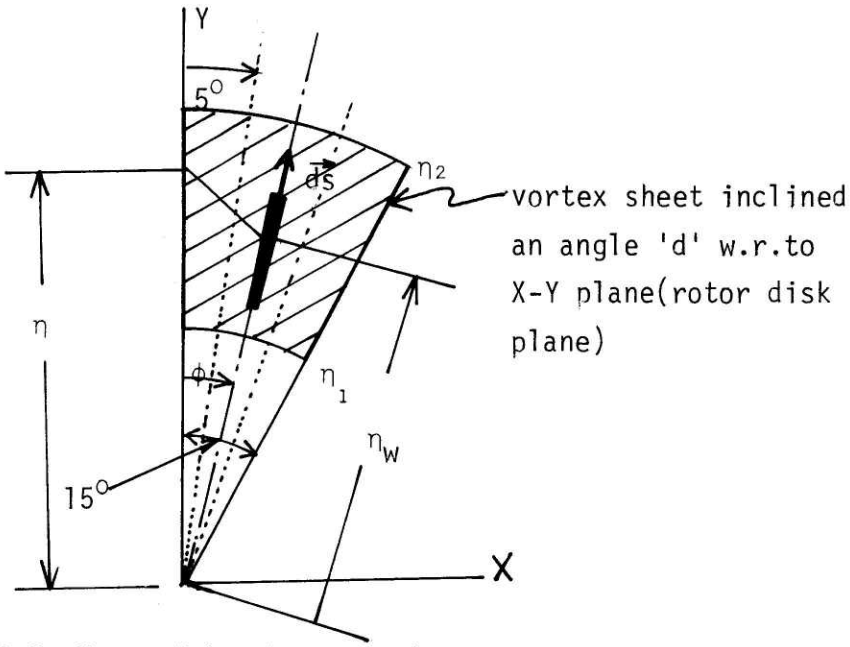

<Fig. A.3> Near Wake Vortex Sheet

$$\vec{dS} = (\sin\phi\,\vec{i} + \cos\phi\,\vec{j} + \tan d\,\vec{k})\,d\eta_w\,\eta_w\,d\phi$$

$$W = -\frac{\Gamma_s}{4\pi}\int_{\phi_1}^{\phi_2}(D\vec{i} + E\vec{k})\,F'\,d\phi = -\frac{\Gamma_s^n}{4\pi}\sum_{n=1}^{3}(D_n\vec{i} + E_n\vec{k})F_n'$$

Here,

$$F' = \left[\frac{B\eta_w + C}{(B-AC)(A\eta_w^2 + 2B\eta_w + C)^{1/2}}\right]_{\eta_w=\eta_1}^{\eta_w=\eta_2}$$

$$A = 1 + \tan^2 d\ ,\quad B = h_o\tan d - \eta\cos\phi\ ,\quad C = \eta^2 + h_o^2\ ,$$

$$D = \eta\tan d + h_o\cos\phi\ ,\quad E = -\eta\sin\phi\ ,\quad \Gamma_s^n = \frac{\Gamma(L+1,N) - \Gamma(L,N)}{\eta_N}$$

The strength of the sheet vortex is $\Gamma_s = \frac{\Gamma(L+1, N) - \Gamma(L, N)}{\eta \Delta \phi}$ where $\Gamma(L,N)$ is bound circulation at the azimuthal position, L and the radial position, N. In this calculation there are no singularities because the integrand is calculated at the midpoint of each section.

Appendix D

WIND PROFILE UP-WIND OF THE TOWER

It is assumed that the free stream undergoes a velocity reduction of the form of a right circular cone on the rotor disk plane due to the up-wind propagation of the tower disturbances. The profile of the disturbed free stream velocity is shown in fig. A.4.

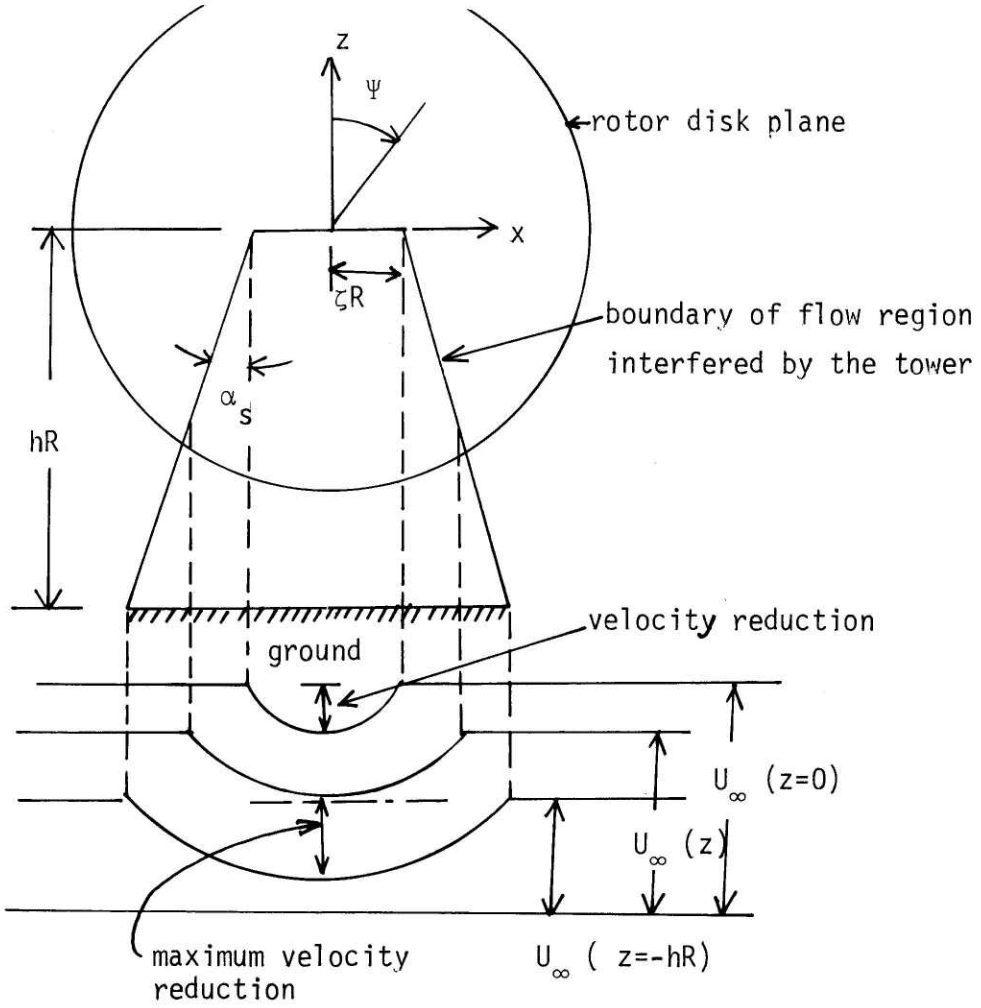

<Fig. A.4> Geometry for the Representation of Tower Reflection Wind Profile

Let v(z) be the maximum velocity reduction function along the height of the tower, and assume v(z) be linear. Then $v(z) = VR \cdot \left\{ 1 - \frac{S_t}{\gamma} \cdot \left(\frac{Z}{R}\right) \right\}$, where $S_t = \tan\alpha_s$, R = rotor radius, and VR = maximum velocity reduction rate at z = 0. The velocity reduction function v(x,z) at an arbitrary point of the flow region up-wind of the tower becomes

$$v(x,z) = \frac{\sqrt{(\gamma - S_t \eta \cos\Psi)^2 - \eta^2 \sin^2\Psi}}{(\gamma - S_t \eta \cos\Psi)} \cdot VR \cdot \left(1 - \frac{S_t}{\gamma} \eta \cos\Psi\right)$$

Therefore, the wind profile behind the tower can be defined by u(x,z) as follows.

(i) $\cos\Psi \geq 0 \Rightarrow u(x,z) = U_\infty(z)/\Omega R$

(ii) $\cos\Psi < 0$ and $\frac{|\gamma - S_t \eta \cos\Psi|}{|\eta \sin\Psi|} \leq 1 \Rightarrow u(x,z) = U_\infty(z)/\Omega R$

$\cos\Psi < 0$ and $\frac{|\gamma - S_t \eta \cos\Psi|}{|\eta \sin\Psi|} > 1 \Rightarrow u(x,z) = \{1 - v(x,z)\} U_\infty(z)/\Omega R$

Here, $U_\infty(z)$ can be a shear flow or a uniform steady flow. In the shear flow case, the velocity reduction function v(x,z) can be assumed to be proportional to the magnitude of free stream. Then, u(x,z) in above last equation is simply modified as follows.

$$u(x,z) = \left\{ 1 - v(x,z) \frac{U_\infty(z=z)}{U_\infty(z=0)} \right\} U_\infty(z=z)/\Omega R$$

For the tower with Xmas tree, v(x,z) is determined from the experimental results.

$$v(x,z) = v_0 z e^{-K|x|}$$

Here, v_0 is the velocity reduction rate at $z = -0.75$ and $x = 0$ and K is the characteristic constant for the given tower. Then the wind profile is

$$u(x,z) = \{1 - v(x,z)\} U_\infty / \Omega R$$

or

$$u(x,z) = \{1 - v(x,z)\frac{U_\infty(z=z)}{U_\infty(z=0)}\} U_\infty(z=z) / \Omega R$$

for shear flow.

v(x,z) is defined as follows.

(i). $z > 0$

$$v(x,z) = v_0 z_x e^{-K|x+z|}$$

(ii). $z_x < z < 0$

$$v(x,z) = v_0 z_x e^{-K|x|}$$

(iii). $z < z_x$

$$v(x,z) = v_0 z e^{-K|x|}$$

z_x is the z-coordinate of the top end of Xmas tree.